Accepted Manuscript

Geological Society, London, Special Publications

A Screening Assessment of the Impact of Sedimentological Heterogeneity on CO_2 Migration and Stratigraphic-Baffling Potential: Sherwood and Bunter Sandstones, UK

Jafar Alshakri, Gary J. Hampson, Carl Jacquemyn, Matthew D. Jackson, Dmytro Petrovskyy, Sebastian Geiger, Julio D. Machado Silva, Sicilia Judice, Fazilatur Rahman & Mario Costa Sousa

DOI: https://doi.org/10.1144/SP528-2022-34

To access the most recent version of this article, please click the DOI URL in the line above. When citing this article please include the above DOI.

Received 18 February 2022
Revised 2 June 2022
Accepted 10 June 2022

A Screening Assessment of the Impact of Sedimentological Heterogeneity on CO_2 Migration and Stratigraphic-Baffling Potential: Sherwood and Bunter Sandstones, UK

Jafar Alshakri[1,2], Gary J. Hampson[1], Carl Jacquemyn[1], Matthew D. Jackson[1], Dmytro Petrovskyy[3,4], Sebastian Geiger[3,4], Julio D. Machado Silva[5], Sicilia Judice[5], Fazilatur Rahman[5] & Mario Costa Sousa[5]

1. Department of Earth Science and Engineering, Imperial College London, London, SW7 2AZ, UK

2. present address: 1st Line Defence, Hertfordshire EN11 0EX, UK

3. Institute of Geoenergy Engineering, Heriot-Watt University, Edinburgh, EH14 4AS, UK

4. Department of Geoscience and Engineering, Delft University of Technology, 2600 AA Delft, The Netherlands

5. Department of Computer Science, University of Calgary, Calgary, TN2 1N4, Canada

E-mail:

g.j.hampson@imperial.ac.uk

ABSTRACT

We use a combination of experimental design, sketch-based reservoir modelling, and flow diagnostics to rapidly screen the impact of sedimentological heterogeneities that constitute baffles and barriers on CO_2 migration in depleted hydrocarbon reservoirs and saline aquifers of the Sherwood Sandstone Group and Bunter Sandstone Formation, UK. These storage units consist of fluvial sandstones with subordinate aeolian sandstones, floodplain and sabkha heteroliths, and lacustrine mudstones. The predominant control on effective horizontal permeability is the lateral continuity of aeolian-sandstone intervals. Effective vertical permeability is controlled by the lateral extent, thickness and abundance of lacustrine-mudstone layers and aeolian-sandstone layers, and the mean lateral extent and mean vertical spacing of carbonate-cemented basal channel lags in fluvial facies-association layers. The baffling effect on CO_2 migration and retention is approximated by the pore volume injected at breakthrough time, which is controlled largely by three heterogeneities, in order of decreasing impact: (1) the lateral continuity of aeolian-sandstone intervals; (2) the lateral extent of lacustrine-mudstone layers, and (3) the thickness and abundance of fluvial-sandstone, aeolian-sandstone, floodplain-and-sabkha-heterolith and lacustrine-mudstone layers. Future effort should be focussed on characterising these three heterogeneities as a precursor for later capillary, dissolution and mineral trapping.

Supplementary material: Rapid Reservoir Modelling prototype (executable and source code) is available at: https://bitbucket.org/rapidreservoirmodelling/rrm. The 32 models used in this study are available at: https://figshare.com/articles/dataset/RRM_models_of_Sherwood_and_Bunter_Sandstones/19210002.

INTRODUCTION

The Triassic Sherwood Sandstone Group and lithostratigraphically equivalent Bunter Sandstone Formation are widely considered for large-scale CO_2 storage in saline aquifers and depleted hydrocarbon reservoirs of the onshore and offshore UK, because of their high storage capacity and favourable injectivity (e.g. Kirk 2005; Holloway et al. 2006; Heinemann et al. 2012; Monaghan et al. 2012; Noy et al. 2012; Williams et al. 2014; Agada et al. 2017). Current storage projects under appraisal include depleted Sherwood Sandstone Group hydrocarbon reservoirs in the Hamilton, Hamilton North and Lennox fields of the Liverpool Bay area, East Irish Sea (https://www.eni.com/en-IT/media/press-release/2020/10/carbon-storage-licence-uk.html) and the

Bunter Sandstone Formation saline aquifer in the Endurance storage site, southern North Sea (Bentham et al. 2017; Gluyas & Bagudu 2020) (Fig. 1). Other hydrocarbon reservoirs in these stratigraphic units also have the potential to be used for future CO_2 storage, including the large Sherwood Sandstone Group reservoir in the Wytch Farm field, southern England (cf. Hogg et al. 2009) (Fig. 1).

To date, CO_2 storage characterisation and modelling studies of the Sherwood Sandstone Group and Bunter Sandstone Formation have focussed largely on storage volumes, aquifer continuity and connectivity, and pressurisation related to fault seal (e.g. Smith et al. 2011; Bricker et al. 2012; Noy et al. 2012; Williams et al. 2013a, 2014; Agada et al. 2017; Bentham et al. 2017). Assessment of the impact of stratigraphic and sedimentological heterogeneities on CO_2 migration and storage has been limited to: (1) the presence or absence of continuous low-permeability layers, (2) variations in the mean porosity and permeability of specific reservoir facies, (3) the sharp or gradational nature of the contact with the overlying seal, and (4) detailed heterogeneity distribution from an outcrop analogue of the contact between the storage unit and seal (Williams et al. 2013a, 2013b; Newell & Shariatipour 2016; Onoja & Shariatipour 2018; Onoja et al. 2019). These studies demonstrate that stratigraphic and sedimentological heterogeneities can act to disperse the plume of injected CO_2 as it migrates, and can create small-scale stratigraphic trapping configurations that increase CO_2 storage efficiency (cf. Flett et al. 2007; Gibson-Poole et al. 2009). However, many additional stratigraphic and sedimentological heterogeneities are documented to occur in the Sherwood Sandstone Group and Bunter Sandstone Formation. The relative impact of different heterogeneity types and distributions on CO_2 migration and storage by stratigraphic trapping remains unclear, as does the impact of different stratigraphic and sedimentological architectures in the Sherwood Sandstone Group and Bunter Sandstone Formation (e.g. Medici et al. 2015, 2017) on the flow behaviour of CO2 storage units.

The aim of this paper is to identify the key stratigraphic and sedimentological heterogeneities that control CO_2 migration and stratigraphic baffling in the Sherwood Sandstone Group and Bunter Sandstone Formation. We address this aim using a screening method that combines experimental design, sketch-based construction of three-dimensional (3D) reservoir models, and flow diagnostics. Sketch-based modelling is implemented in open source research code (Rapid Reservoir Modelling, RRM) that is designed to be geologically intuitive and does not require specialist reservoir modelling experience (Costa Sousa et al. 2020; Jacquemyn et al. 2021a), and that is integrated with computationally cheap flow diagnostics (Zhang et al. 2017, 2020; Jacquemyn et al. 2021b; Petrovskyy et al. in review). The method allows a large number of geological scenarios to be explored in a fast, efficient manner prior to more detailed flow simulation.

GEOLOGICAL BACKGROUND

The Sherwood Sandstone Group and Bunter Sandstone Formation both consist of fluvial sandstones with subordinate aeolian sandstones, floodplain and sabkha heteroliths, and lacustrine mudstones (e.g. Cooke-Yarborough 1991; Ketter 1991; Meadows & Beach 1993a, 1993b; Ritchie & Pratsides 1993; McKie et al. 1998; Meadows 2006; Brookfield 2008; McKie & Williams 2009; Medici et al. 2015; Wakefield et al. 2015; Newell 2018a, 2018b). The Sherwood Sandstone Group and Bunter Sandstone Formation are overlain by the thick, evaporite-bearing lacustrine mudstones of the Mercia Mudstone Group and Haisborough Group, respectively.

During the Triassic, the UK lay in the eastern, internal part of the Pangean supercontinent, and occupied a palaeo-latitude of 15-25°N (e.g. Ziegler 1991; McKie & Williams 2009; Newell 2018b). The remnants of the Variscan Mountains lay to the south of the UK, and separated it from the Tethys Ocean. The major river systems that deposited much of the Sherwood Sandstone Group and Bunter Sandstone Formation were derived from the remnants of the Variscan Mountains, and flowed north through a series of linked continental rift basins (McKie & Williams 2009; Tyrell et al. 2012; Morton et al. 2013, 2016; Newell 2018b). Additional sediment was supplied by local rivers that drained the flanks of these rift basins (Tyrell et al. 2012; Morton et al. 2013, 2016). Aeolian sandstones generally record transport and reworking by westward-directed trade winds (Meadows & Beach 1993a; McKie & Williams 2009; Newell 2018b), and become progressively more common towards the north and west of the UK (e.g. Medici et al. 2019). The assemblage of depositional facies in the Sherwood Sandstone Group and Bunter Sandstone Formation is interpreted to record deposition under arid and semi-arid conditions (e.g. Meadows & Beach 1993a, 1993b; McKie et al. 1998; Meadows 2006; Brookfield 2008; Medici et al. 2015; Wakefield et al. 2015). However, facies architecture indicates perennial flow in the major, trunk rivers, implying intense Tethyan-monsoonal precipitation over the remnants of the Variscan Mountains (e.g. McKie & Williams 2009; Medici et al. 2015; Newell 2018a,

2018b). The presence of evaporites, including locally thick halite deposits, in the Mercia Mudstone Group and Haisborough Group, supports deposition in an arid to semi-arid climate. Alternations between fluvial and aeolian deposits, between perennial and ephemeral fluvial deposits, and between playa-lacustrine and fluvial deposits are interpreted to record temporal variations between more humid (wetter) and more arid (dryer) climate (e.g. Meadows & Beach 1993a; McKie & Williams 2009; Newell 2018a). The preservation of these facies-association alternations is influenced locally by tectonic subsidence (e.g. McKie & Williams 2009; Newell 2018a).

Sedimentological heterogeneity in the Sherwood Sandstone Group and Bunter Sandstone Formation

We synthesise previous sedimentological studies of the Sherwood Sandstone Group and Bunter Sandstone Formation at outcrop and in the subsurface (Fig. 1) to define a hierarchy of heterogeneity in these units (Fig. 2). This hierarchy is used to define input values for numerical reservoir models in our screening assessment.

At the scale of the sedimentary basins that contain the Sherwood Sandstone Group and Bunter Sandstone Formation, the principal heterogeneity is the inferfingering of lithostratigraphic units that comprise fluvial and aeolian sandstones, floodplain and sabkha heteroliths, and lacustrine mudstones (Fig. 2A). This interfingering reflects a combination of: tectonic subsidence, which controlled stratal thickness and the distribution of unconformities and related lithostratigraphic units (McKie & Williams 2009; Newell 2018a); sediment routing into the basins, which controlled the distribution of trunk river systems and dispersal of the sediment and water that they discharged (Tyrell et al. 2012; Morton et al. 2013, 2016; Medici et al. 2015); and climatic variations in humidity and aridity, which controlled fluvial discharge and lake extent (Meadows & Beach 1993a; McKie & Williams 2009; Newell 2018a).

At the scale of individual reservoirs and storage units, basin-scale interfingering of lithostratigraphic units is expressed in the thickness of layers of fluvial sandstones, aeolian sandstones, floodplain and sabkha heteroliths, and lacustrine mudstones (Ketter 1991; Meadows & Beach 1993a; Ritchie & Pratsides 1993; Jones & Ambrose 1994; McKie et al. 1998; Mountney & Thompson 2002; Meadows 2006; Medici et al. 2015; Wakefield et al. 2015; Newell 2018a) (Fig. 2B). In southerly basins that are proximal to the source of trunk rivers, fluvial sandstone layers are thick and intervening layers of aeolian, floodplain, sabkha and lacustrine deposits are thin and scarce (e.g. in the Wessex Basin of southern England; McKie et al. 1998; Newell 2018a; Medici et al. 2019). In northerly, distal basins, fluvial sandstone layers are thin and intervening layers of aeolian, floodplain, sabkha and lacustrine deposits are thick and abundant (e.g. in the East Irish Sea Basin; Meadows & Beach 1993a; Yaliz & Chapman 2003; Meadows 2006; Medici et al. 2019). The lateral continuity of aeolian-sandstone and

lacustrine-mudstone layers in reservoirs and storage units vary accordingly. For example, aeolian sandstones may occur as laterally continuous sheets or discontinuous lenses (McKie et al. 1998; Meadows & Beach 199a; Yaliz & Chapman 2003; Meadows 2006), while lacustrine-mudstone sheets may extend across or pinch out in a reservoir or storage unit (McKie et al. 1998; Meadows 2006) (Fig. 2B).

Within reservoirs and storage units, smaller scale heterogeneities occur within layers of fluvial sandstones, aeolian sandstones, floodplain and sabkha heteroliths, and lacustrine mudstones (Figs. 2B, C, 3). Layers of floodplain and sabkha heteroliths contain channelised fluvial sandbodies and non-channelised sheetflood sandbodies (Ketter 1991; Bowman et al. 1993; Meadows & Beach 1993a; Ritchie & Pratsides 1993; McKie et al. 1998; Medici et al. 2015; Newell 2018a) (Figs. 2B, 3A, D). The proportion of channelised fluvial sandbodies, their connectivity, and the geometry and extent of sheetflood sandbodies may all vary in these layers (McKie et al. 1998). Fluvial-sandstone layers comprise vertically and laterally stacked channelised fluvial sandbodies, with rare channel-plug mudstones and preserved remnants of floodplain heteroliths (Ketter 1991; Bowman et al. 1993; Ritchie & Pratsides 1993; Lorsong & Atkinson 1995; McKie et al. 1998; Medici et al. 2015; Wakefield et al. 2015) (Fig. 2C). Channelised fluvial sandbodies in these layers vary in their preserved dimensions, reflecting differences in river channel mobility and tectonic subsidence rate, and in their internal facies architecture, reflecting differences in river discharge regime and sediment calibre (McKie et al. 1998; Medici et al. 2015). Thus, heterogeneities in fluvial-sandstone layers include the: abundance, lateral extent and vertical spacing of carbonate-cemented basal channel lags (Dranfield et al. 1987; Bowman et al. 1993; Lorsong & Atkinson 1995; Newell 2006; Fig. 3A, B); the vertical and lateral succession of facies (e.g. grain size and sedimentary structures) in each channelised sandbody (Dranfield et al. 1987; Ketter 1991; Bowman et al. 1993; Lorsong & Atkinson 1995; Medici et al. 2015; Wakefield et al. 2015; Newell 2018a; Fig. 3B); and the abundance, dimensions and distribution of channel-plug mudstones and preserved remnants of floodplain heteroliths (Dranfield et al. 1987; Bowman et al. 1993; Lorsong & Atkinson 1995; Medici et al. 2015; Fig. 3C) (Fig. 2C). Heterogeneities in aeolian-sandstone layers reflect differences in the stacking of wind-blown sand dunes and their interaction with waterlain, interdune muds and sands (Mountney & Thompson 2002).

Smaller-scale heterogeneities (at centimetre to metre scales) related to sedimentary structures occur within the facies components of channelised fluvial sandbodies, sheetflood sandbodies, aeolian cross-bedded sandstones, and other lithological elements. Figure 2 does not portray these heterogeneities. At even smaller scales, sub-centimetre heterogeneities reflect grain-size distributions, sorting and textures, together with cementation. Heterogeneities at this scale control porosity, permeability and relative permeability. Aeolian sandstones are better sorted and have lower clay

contents than fluvial sandstones, and thus are characterised by higher values of porosity and permeability (Meadows & Beach 1993b; Hogg et al. 1996; Bloomfield et al. 2006). Where their grain-size characteristics and texture indicate reworking from aeolian sands, sheetflood sandstones have porosity and permeability values that are intermediate between those of aeolian and fluvial sandstones (Meadows & Beach 1993b); in contrast, sheetflood sandstones have lower porosity and permeability values than fluvial sandstones where their grain-size characteristics and texture indicate reworking and dispersal of fluvially supplied sand (Hogg et al. 1996). Floodplain and lacustrine mudstones are considered to be non-reservoir lithologies (Ketter 1991; Ritchie & Pratsides 1993; McKie et al. 1998).

METHODOLOGY

We use a screening approach to assess the influence of sedimentological heterogeneities that constitute baffles and barriers on CO_2 migration in the Sherwood Sandstone Group and Bunter Sandstone Formation. We do not explicitly model the storage unit at any specific site, but instead investigate the influence of heterogeneities that are generic to all storage sites. We use a method combining three key elements: (1) experimental design, which allows efficient exploration of a wide parameter space; (2) sketch-based reservoir modelling, which enables rapid construction of deterministic models of interpreted geological scenarios, and (3) flow diagnostics, which provide computationally cheap approximations of full-physics, multiphase simulations that are reasonable for many subsurface-flow conditions. These three elements and other aspects of the modelling methods are described below. Integrated sketch-based reservoir modelling and flow diagnostics are implemented in open source research code (Rapid Reservoir Modelling, RRM; Zhang et al. 2017, 2020; Costa Sousa et al. 2020; Jacquemyn et al. 2021a, 2021b; Petrovskyy et al. in review). Our approach is scenario-based and deterministic (Bentley & Smith 2008), and it is appropriate for screening the most influential sedimentological heterogeneities prior to more detailed follow-up studies, including stochastic modelling of selected scenarios.

Design of modelling experiment

Based on previous descriptions of the sedimentological character of the Sherwood Sandstone Group and Bunter Sandstone Formation (as synthesised in Fig. 2), we selected eight sedimentological heterogeneities for investigation (Table 1). Established experimental design techniques (Box et al. 1978; Damsleth et al. 1992; Kjønsvik et al. 1994; White & Royer 2003) were used to efficiently explore the resulting parameter space. 256 (i.e. 2^8) modelling scenarios would be developed for all combinations of the eight selected heterogeneities, if each heterogeneity was assigned either a high or low setting, in a full-factorial design. This large number of modelling scenarios is considered to be too time-consuming for a screening assessment. Instead, we used a two-level fractional-factorial design

(2_{IV}^{8-3}) in which each factor (heterogeneity) is assigned either a low or high setting. Settings are chosen to represent contrasting, but realistic, values for each heterogeneity in the various Sherwood Sandstone Group and Bunter Sandstone Formation potential storage units (Table 1). The experimental design allows us to efficiently quantify the effect of varying each factor from its low setting to its high setting. The resolution IV design ensures that the main effects, due to each of the eight studied heterogeneities, are not confounded with interactions between two heterogeneities (Box et al. 1978). The experimental design requires only 32 models to be constructed for the screening study (Table 2). This experimental design allows the eight selected heterogeneities to be ranked robustly, based on the average response of a given metric across the ensemble of 32 models. However, additional modelling scenarios would be required to characterise the effects of interactions between two or more heterogeneities, the effects of heterogeneity settings that lie between their high and low settings, and the effects of additional heterogeneities.

Modelled heterogeneities and settings

The eight sedimentological heterogeneities under investigation are listed below in order of decreasing length scale (Fig. 2). Their settings are explained below and summarised in Table 2. All models contain a repeated succession of facies-association layers consisting of, from base to top: (1) aeolian sandstone; (2) fluvial sandstone; (3) floodplain and sabkha heteroliths; and (4) capping alternate successions, lacustrine mudstone (Fig. 4). Thus models contain one layer of lacustrine mudstone for every two layers of fluvial sandstone, aeolian sandstone, and floodplain and sabkha heteroliths. The porosity and permeability values assigned to each facies association in the models (Fig. 2B) are listed in Table 3. Absolute values of porosity and permeability differ depending on diagenetic history and burial depth (Burley 1984), but the relative differences between facies associations remain similar (e.g. Meadows & Beach 1993b; Hogg et al. 1996; Bloomfield et al. 2006). We assign lower porosity and permeability values to sheetflood sandstones than to fluvial sandstones on the assumption that the former were derived from, and are thus finer-grained textural equivalents of, the latter (cf. Hogg et al. 1996).

The thickness of facies-association layers (i.e. layers of fluvial sandstones, aeolian sandstones, floodplain and sabkha heteroliths, lacustrine mudstones; Fig. 2B) varies between different Triassic basins that contain storage sites. Fluvial-sandstone layers, consisting of vertically and laterally stacked channelised fluvial sandbodies, form sheets that vary in thickness from 5 to 35 m in the Wessex Basin, including in the Wytch Farm oilfield (McKie et al. 1998; Newell 2018a), 5 to 40 m in the East Irish Sea Basin, including in the Liverpool Bay oil and gas fields (Meadows & Beach 1993a; Yaliz & Chapman 2003; Meadows 2006), and 5 to 65 m in the southern North Sea, including the Caister, Esmond, Forbes and Gordon gas fields (Ketter 1991; Ritchie & Pratsides 1993). Aeolian sandstones

occur as discontinuous sheets and lenses up to 15 m thick in the Wessex Basin (McKie et al. 1998; Newell 2018a), discontinuous sheets 5-30 m thick in the East Irish Sea Basin (Meadows & Beach 1993a; Yaliz & Chapman 2003; Meadows 2006), and are absent in the Bunter Sandstone gas fields of the southern North Sea (Ketter 1991; Ritchie & Pratsides 1993). Floodplain and sabkha heteroliths form sheets of varying continuity that are 5-20 m thick in the Wessex Basin (McKie et al. 1998; Newell 2018a), 5-10 m thick in the East Irish Sea Basin (Meadows & Beach 1993a; Yaliz & Chapman 2003; Meadows 2006), and 10-20 m thick in the Bunter Sandstone gas reservoirs of the southern North Sea (Ketter 1991; Ritchie & Pratsides 1993). Lacustrine-mudstone layers occur as thin (<10 m) sheets in all three basins (Ketter 1991; Ritchie & Pratsides 1993; Meadows & Beach 1993a; McKie et al. 1998; Yaliz & Chapman 2003; Meadows 2006; Newell 2018a). Based on these thickness ranges, we select the following values for low and high settings of facies-association layers: 10 and 40 m for fluvial sandstones; 5 and 25 m for aeolian sandstones; 5 and 20 m for floodplain and sabkha heteroliths; and 2 and 5 m for lacustrine mudstones (Table 1). These are not extreme end-member values, but represent values that can occur in potential storage sites in most offshore and onshore UK basins (Fig. 1). We choose to include aeolian sandstones in all our models, even though they are not interpreted in the Bunter Sandstone gas reservoirs of the southern North Sea (Ketter 1991; Ritchie & Pratsides 1993); the latter unit is sparsely sampled by core, so that it remains possible that Bunter Sandstone saline aquifers contain aeolian sandstones (Gluyas & Bagudu 2020). Our models all have a uniform thickness (176 m), such that they either contain a small number of thick facies-association layers or a large number of thin facies-association layers (Fig. 5).

The lateral continuity of aeolian-sandstone layers is varied between a low setting of discontinuous lenses of areal extent c. 350 m x 170 m and a high setting of continuous sheets (Table 1; Figs. 2B, 5). These low and high settings are consistent, respectively, with observations from the Wytch Farm oilfield in the Wessex Basin (McKie et al. 1998) and the Liverpool Bay oil and gas fields in the East Irish Sea Basin (Meadows & Beach 1993a; Yaliz & Chapman 2003; Meadows 2006). The lateral continuity of lacustrine-mudstone layers is also varied between a low setting of discontinuous sheets, representing the marginal pinch-out of a playa lake, and a high setting of continuous sheets (Table 1; Figs. 2B, 5). Fluvial-sandstone layers and floodplain-and-sabkha-heterolith layers are represented as continuous sheets in all models (Fig. 5).

The proportion of channelised fluvial sandbodies in floodplain-and-sabkha-heterolith layers (Fig. 2B) is varied between low and high settings of approximately 17% and 33% (Table 1). Channelised fluvial sandbodies are modelled as single-storey units with widths and thicknesses of c. 20 m and c. 5-10 m, respectively. The number of these bodies is doubled in models with the high setting, relative to models with the low setting. The connectivity of these channelised fluvial sandbodies is varied by

changing their plan-view geometry and spacing, between: (1) several clusters of 2-3 connected channelised sandbodies that are isolated from other clusters in the low setting; and (2) in the high setting, intersecting clusters of 2-3 channelised sandbodies that form a laterally connected network of channelised sandbodies over the entire model area (Table 1). All channelised fluvial sandbodies are modelled as having low sinuosities (1.03-1.15) and uniform widths in plan view. The geometry of sheetflood sandbodies, which also have the potential to connect channelised fluvial sandbodies in floodplain-and-sabkha-heterolith layers (Fig. 2B), is varied between a high setting of discontinuous lenses c. 150 m wide and a low setting of continuous sheets (Table 1). In the high setting, lenticular sheetflood sandbodies extend across the width of two channelised fluvial sandbodies that cut into them, and then thin to their lateral pinchouts. The sheetflood sandbodies have straight pinchouts in plan view, and thus maintain a uniform cross-sectional geometry in the third dimension (i.e. parallel to the mean centreline position of the two channelised fluvial sandbodies). In the high setting, sheetflood sandbodies form continuous sheets of approximately uniform thickness that are cut into by all channelised fluvial sandbodies developed at the same stratigraphic level. The proportions, thicknesses and widths of channelised fluvial sandbodies and sheetflood sandbodies for the various settings described above are generally consistent with those documented at outcrop and interpreted in closely spaced wells in the Sherwood Sandstone Group and Bunter Sandstone Formation (e.g. Meadows & Beach 1993a; McKie et al. 1998; Medici et al. 2015).

In fluvial-sandstone layers, we vary the mean vertical spacing and mean lateral extent of carbonate-cemented lags at the base of channelised fluvial sandbodies (Fig. 2C) in order to reflect variations in the depositional geometry, stacking and preservation of such sandbodies. Outcrops and subsurface cores of the Sherwood Sandstone Group in the Wessex Basin (e.g. Fig. 3A, B) indicate that representative vertical spacing varies between low and high settings of 2 and 10 m, respectively, and representative lateral extent between low and high settings of 8 and 20 m, respectively (Dranfield et al. 1987; Bowman et al. 1993; Lorsong & Atkinson 1995; Newell 2006; Table 1). More laterally extensive carbonate-cemented basal lags resulting from pronounced multilateral stacking of channelised fluvial sandbodies (Lorsong & Atkinson 1995; Newell 2006) are excluded from our estimates. The low- and high-setting values of mean lateral extent and vertical spacing are used to estimate k_v/k_h ratio using the statistical derivation of Begg & King (1985), also applied by Dranfield et al. 1987), and assuming that vertical permeability is equal to horizontal permeability in the intervening sandstones:

$$k_v/k_h = (1 - F_s) / \{1 + s * (l / 3)\}^2 \quad (1)$$

where F_s is the fraction of cemented lag, s is the inverse of the mean vertical spacing of cemented lags, and l is the mean length of cemented lags. F_s is assigned a value of 0.07 (after Bowman et al. 1993; Lorsong & Atkinson 1995). The resulting estimates of permeability anisotropy (k_v/k_h ratio) that account for variations in the distribution and extent of carbonate-cemented basal channel lags are: (1) 0.16 for the low settings of both mean vertical spacing and mean lateral extent; (2) 0.05 for the low setting of mean vertical spacing and high setting of mean lateral extent; (3) 0.57 for the high setting of mean vertical spacing and low setting of mean lateral extent; and (4) 0.33 for the high settings of both mean vertical spacing and mean lateral extent. Basal channel lags in the East Irish Sea Basin and southern North Sea are more rarely carbonate cemented (Ketter 1991; Meadows & Beach 1993a; Yaliz & Chapman 2003; Gluyas & Bagudu 2020), but may contain abundant mudstone clasts that result in low permeabilities (Ketter 1991).

Sketch-based construction of reservoir models

We use an intuitive, sketch-based approach that adapts generic Sketch-Based Interface and Modelling (SBIM) methods to construct the reservoir models. In this approach, all geological architectures and heterogeneities (e.g. stratigraphic surfaces, facies-association boundaries, sandbody boundaries) are represented by surfaces that define and bound geological domains (cf. Pyrcz et al. 2005; Caumon et al. 2009; Sech et al. 2009; Ruiu et al., 2016; Jacquemyn et al., 2019). Since surfaces and surface-bounded geological domains are widely used by geoscientists to conceptualise and represent geological interpretations (e.g. in maps, cross-sections and block diagrams; e.g. Fig. 2) and can be generated and manipulated using SBIM methods, with geological viability enforced in the resulting models by operator-controlled interactions between SBIM-generated surfaces, using our sketch-based modelling approach allows non-expert users to capture geological concepts and scenarios (Costa Sousa et al. 2020; Jacquemyn et al. 2021a).

32 models were constructed, following the experimental design (Table 2). In this study, models were sketched following the hierarchy of heterogeneity (Fig. 2), with heterogeneities at large length scales sketched first, followed by heterogeneities at progressively smaller length scales. Six heterogeneities were sketched explicitly in the models: (1) thickness of facies-association layers; lateral continuity of (2) aeolian and (3) lacustrine facies-association bodies; (4) proportion and (5) connectivity of channelised fluvial sandbodies, and (6) lateral continuity of sheetflood sandbodies in floodplain-and-sabkha facies-association layers (Table 1). Different heterogeneities are sketched in different ways (Costa Sousa et al. 2020; Jacquemyn et al. 2021a, 2021b). For example, laterally discontinuous lacustrine-mudstone sheets and sheetflood sandbodies (e.g. Figs. 4, 5A, B) are sketched in a single vertical cross-section, and their cross-sectional geometry is then extruded linearly into the third dimension. Channelised fluvial sandbodies (Figs. 4, 5A) are sketched in a single vertical cross-section,

and their cross-sectional geometry is then extruded along a sketched plan-view trajectory. Laterally discontinuous aeolian-sandstone lenses (Figs. 4, 5B) are constructed by extrapolating between contours sketched on a series of plan-view maps. Where combinations of the same settings for these heterogeneities recur in different models, the surfaces that represent these heterogeneities were re-used in order to maintain consistency in geological-domain geometries and volumes. Two further heterogeneities, which occur at relatively small length scales, were represented implicitly by assigning different values of permeability anisotropy (k_v/k_h) to geological domains: (7) mean vertical spacing and (8) mean lateral extent of carbonate-cemented basal channel lags in fluvial facies-association layers (Table 1). Since these two heterogeneities are not explicitly represented by sketched surfaces, their setting does not affect geological-domain geometries and volumes.

Each model has dimensions of 600 m (west-east) x 600 m (north-south) x 176 m (thickness) (Fig. 4). The areal extent of the models is thus significantly smaller than that of the Endurance storage site (140 km^2; Gluyas & Bagudu 2020), the Hamilton, Hamilton North and Lennox gas fields (respectively 15 km^2, 8 km^2 and 9 km^2; Yaliz & Chapman 2003; Yaliz & Taylor 2003) and the Wytch Farm Field (20 km^2; Bowman et al. 1993) (Fig. 1). The thickness of the models is comparable to that of the Bunter Sandstone Formation in the Endurance storage site (275 m; Gluyas & Bagudu 2020) and the Sherwood Sandstone Group in the Wytch Farm Field (150 m; McKie et al. 1998), although the Sherwood Sandstone Group is considerably thicker in the East Irish Sea Basin (>1000 m; Meadows & Beach 1993a). The models are intended to investigate only a representative part of the potential storage units and sites, at a spatial scale that captures the heterogeneities under investigation. Structural elements of specific storage sites, including faults and tectonic dip, are not incorporated in the models. Depending on the heterogeneity settings for each model, they contain 25 to 115 geological domains. Models are generated without reference to an underlying grid, although a grid is created to visualise them (Fig. 4) or to perform numerical calculations (Zhang et al. 2018).

Architectures modelled in floodplain-and-sabkha-heterolith layers were simplified in three ways, due to practical constraints. (1) Single-storey channelised fluvial sandbodies are narrower (c. 20 m; Figs 4, 5) than those documented at outcrop (c. 50 m to >75 m; Medici et al. 2015; Newell & Shariatipour 2016), in order that we could incorporate variations in sandbody connectivity due to low and high settings of channelised sandbody proportions, channelised sandbody connectivity and sheetflood sandbody ccontinuity in the areal extent of the models (600 m x 600 m). (2) Some (but not all) of the channelised fluvial sandbodies developed at a single stratigraphic horizon are sketched with one west-to-east cross-section line and plan-view trajectory, which defines the geometries and lateral spacing of these sandbodies. The other channelised fluvial sandbodies developed at the same stratigraphic horizon are sketched with a second cross-section line and plan-view trajectory. This

approach allows sandbody intersections and connectivity to be defined using only two surfaces, but results in sets of channelised sandbodies that are parallel to each other in plan view (Figs 4, 5). (3) Discontinuous sheetflood sandbodies developed at a single stratigraphic horizon are modelled using one west-to-east cross-section line and then extruded linearly in the south-to-north orientation. The resulting sandbodies do not intersect with each other, but do not follow the sinuous plan-view trajectory of the channelised fluvial sandbodies that cut into them. As a result of these three simplifications, details of the modelled architectures in floodplain-and-sabkha-heterolith layers in some models may appear unrealistic; however the models capture a range of sandstone proportions and sandbody connectivities that are consistent with the interpreted sedimentological scenarios.

Flow diagnostics

Models can be visually inspected to assess that stratigraphic architecture is represented as intended by the user in the sketch-based models (e.g. Fig. 4B). The pore volume of the models can be calculated after porosity values have been assigned to the facies associations in geological domains (Table 3). Flow diagnostics allow key flow properties and behaviours to be assessed by solving a single-phase, steady-state pressure field for a given combination of fluid injection and offtake (production) wells (Shahvali et al. 2012; Møyner et al. 2014). As a result, tracer flow paths and "time-of-flight" through connected, highly permeable facies associations are highlighted, and parameters such as effective permeability, Lorenz coefficient, sweep efficiency and storage efficiency can be calculated (Møyner et al. 2014). The effects of fluid compressibility, transient flow (e.g. gravity segregation), multiphase fluid interaction (e.g. dissolution) and fluid-rock interactions (e.g. mineralisation) are not included in flow diagnostics. We use flow diagnostics to make a rapid, preliminary assessment of the impact of different geological concepts and scenarios on flow properties and behaviours, as a precursor to more detailed but time-consuming full-physics, multiphase simulations (Zhang et al. 2017, 2020; Jacquemyn et al. 2021b; Petrovskyy et al. in review). A full treatment of our implementation of flow diagnostics is given in Petrovskyy et al. (in review).

Volumetric calculations require a grid to be generated for the models, and flow-diagnostic calculations additionally require specification of boundary conditions and the number, location, perforation interval and bottom-hole pressure of injection and offtake wells. An orthogonal grid is used, to ensure numerical stability. Grid cells measure 6.0 m (west-east) x 6.0 m (north-south) x 1.8 m (thickness), and there are 10^6 grid cells in each model. This grid resolution is sufficiently fine to preserve the geometry and continuity of small geological domains (e.g. single-storey channelised fluvial sandbodies and sheetflood sandbodies; Fig. 4B), and to calculate flow diagnostics with reasonable accurately, based on sensitivity tests. The faces of each model are set as no-flow boundaries. A single vertical injection well and a single vertical offtake well are placed in the centre of

opposing model faces, with both wells perforated over the entire model thickness and the pressure differential between injection and offtake wells set at 50 bar (Fig. 4C). Flow is simulated from south to north (i.e. parallel to the pinchout of lacustrine-mudstone layers, subparallel to the centrelines of sheetflood and channelised fluvial sandbodies in floodplain-and-sabkha-heterolith layers, and along the short axis of aeolian-sandstone lenses; coloured blue in Fig. 4C), and from west to east (i.e. perpendicular to the pinchout of lacustrine-mudstone layers, subperpendicular to the centrelines of sheetflood and channelised fluvial sandbodies in floodplain-and-sabkha-heterolith layers, and along the long axis of aeolian-sandstone lenses; coloured red in Fig. 4C). These well placements, perforations and bottom-hole pressure constraints are not indicative of the development plan for any storage site, but are instead chosen to investigate fluid migration and potential retention over the length scale of the model volume.

Volumetric and flow-diagnostic calculations for different models are compared using four metrics: (1) total pore volume, which describes the maximum potential for fluid storage; (2) effective permeability, computed for the model volume in three major directions (x, y, z) using flow-based upscaling with no-flow boundaries; (3) Lorenz coefficient, which describes the degree of heterogeneity under dynamic conditions within the storage unit; and (4) pore volume injected at breakthrough time, which provides a measure of how much injected fluid is stored in the model volume as a result of stratigraphic baffling and trapping. The Lorenz coefficient is calculated from the cumulative frequency distributions of mean effective permeability in the x and y directions (k_x, k_y) in horizontal layers of the models, and varies between 0 for a homogeneous unit and 1 for a completely heterogeneous unit (Schmalz & Rahme 1950). The Lorenz coefficient and pore volume injected at breakthrough time are calculated for both west-to-east and south-to-north tracer flow (coloured red and blue, respectively, in Fig. 4C). Since flow diagnostics are calculated for tracer flow, values of pore volume injected at breakthrough time do not account for residual water saturation; these values are systematic overestimates, but are appropriate as indicative values for screening purposes.

RESULTS

Stratigraphic architectures

Visual inspection of the sketch-based models (e.g. Figs. 4B, 5) indicates that modelled stratigraphic architectures are consistent with the geological concepts and data on which they are based (Fig. 2A, B). These modelled architectures reflect the sequence and lateral continuity of facies-association layers together with the proportion, distribution and geometry of sheetflood and channelised fluvial sandbodies in floodplain-and-sabkha-heterolith layers (Table 2).

Total pore volume

Values of total pore volume in the suite of 32 models range from 9.9 x 10^6 m^3, equivalent to an average porosity of 15.6% (model number 22; Table 2), to 11.0 x 10^6 m^3, equivalent to an average porosity of 17.3% (model number 11; Table 2), with a mean value of 10.5 x 10^6 m^3 (equivalent to an average porosity of 16.6%). The lateral continuity of aeolian-sandstone bodies has the largest impact on total pore volume (7%; Fig. 6), because this controls the volume of the most porous facies association (Table 3). The thickness of facies association layers has the second largest impact (2%; Fig. 6), whereas all other heterogeneities and the confounded interactions of multiple heterogeneities have only a small effect (<1%; Fig. 6). Overall, the total pore volume of the models is relatively uniform.

Effective permeability

Effective permeability at the scale of the model volume is anisotropic. Mean values of effective permeability in the suite of models are 830 mD, 820 mD and 20 mD in the west-east (k_x), north-south (k_y) and vertical (k_z) orientations, respectively.

The lateral continuity of aeolian-sandstone bodies has by far the largest impact on both k_x and k_y (61% and 66%, respectively; Fig. 7A). Discontinuous aeolian-sandstone lenses (low setting; Table 1) do not extend across the model volume in either a west-east or north-south orientation, in contrast to continuous aeolian-sandstone sheets (high setting; Table 1). The resulting discrepancy in the connectivity between opposing model faces of high-permeability aeolian sandstones accounts for the large effect on k_x and k_y. All other heterogeneities, and the confounded interactions of multiple heterogeneities, have a much smaller effect (<7%; Fig. 7A).

In contrast, multiple heterogeneities control k_z. The two heterogeneities with the largest effects are the lateral continuity of lacustrine mudstones (93%; Fig. 7B) and the thickness of facies-association layers (76%; Fig. 7B). Both parameters influence the tortuosity of vertical flow paths around low-permeability lacustrine-mudstone and floodplain-mudstone baffles (Table 3), because they control the lateral extent and the number of such baffles. The effects of mean lateral extent and mean vertical spacing of carbonate-cemented channel lags in fluvial-sandstone layers are also influential (47% and 37%; Fig. 7B); these two heterogeneities control vertical flow-path tortuosity in fluvial-sandstone layers (Begg & King 1985). The lateral continuity of aeolian-sandstone bodies has a significant effect (41%; Fig. 7B), as does the proportion of channelised fluvial sandbodies in layers of floodplain-and-sabkha heteroliths (26%; Fig. 7B). Both of these heterogeneities control the number of vertical flow paths through relatively low-permeability layers. The confounded effects of interacting heterogeneities, for example those of the lateral continuity of lacustrine mudstones in combination with the thickness of facies-association layers, may also be important (up to 48%; Fig. 7B).

Lorenz coefficient

Values of the Lorenz coefficient are similar for south-to-north displacements (mean of 0.40, and range of 0.27-0.50) and west-to-east displacements (mean of 0.42, and range of 0.34-0.50) in the suite of models. The models therefore exhibit a similar degree of heterogeneity in north-south and west-east orientations.

The lateral continuity of aeolian-sandstone bodies has the largest impact on the Lorenz coefficient (44% and 25% in north-south and west-east orientations, respectively; Fig. 8), while the thickness of facies-association layers has the second largest impact (8% and 12% in north-south and west-east orientations, respectively; Fig. 8). The effects of other individual heterogeneities and the confounded effects of interacting heterogeneities are minor (<2%; Fig. 8).

Pore volume injected at breakthrough time

Mean values of pore volume injected at breakthrough time are similar for south-to-north displacements (mean of 0.59, and range of 0.49-0.76) and west-to-east displacements (mean of 0.54, and range of 0.44-0.73) in the suite of models. These values provide an indication of the effects of stratigraphic baffling and trapping on CO2 migration and retention, but they do not correspond directly to values of storage efficiency.

The three individual heterogeneities with the largest impact on pore volume injected at breakthrough time are: (1) the lateral continuity of aeolian-sandstone bodies (29% and 17% in north-south and west-east orientations, respectively; Fig. 9); (2) the lateral continuity of lacustrine-mudstone bodies (5% and 9% in north-south and west-east orientations, respectively; Fig. 9); and (3) the thickness of facies-association layers (1% and 13% in north-south and west-east orientations, respectively; Fig. 9). Other individual heterogeneities have small effects in both north-south and west-east orientations (<6%; Fig. 9). The confounded effects of interacting heterogeneities are also significant (up to 7% and 20% in north-south and west-east orientations, respectively; Fig. 9).

IMPLICATIONS FOR SHERWOOD AND BUNTER SANDSTONE STORAGE UNITS AND STORAGE SITES

Our results indicate that effective permeability (k_x, k_y, k_z), the Lorenz coefficient, and pore volume injected at breakthrough time are controlled by three heterogeneities, for the settings chosen in this study (Table 1): (1) the lateral continuity of aeolian-sandstone bodies; (2) the lateral continuity of lacustrine-mudstone bodies; and (3) the thickness of facies-association layers (Figs. 7, 8, 9). Preferential flow through thick, high-permeability aeolian sandstones is evident in simulated tracer flow saturations that are visualised at different times (e.g. Fig. 10). In addition, k_z is controlled by the mean lateral extent and mean vertical spacing of carbonate-cemented channel lags in fluvial-sandstone layers (Fig. 7B). These results are consistent with production data from the Sherwood

Sandstone Group reservoirs of the Wytch Farm oilfield and the Bunter Sandstone Formation reservoirs of southern North Sea gas fields, in which thin lacustrine mudstones of varying lateral extent act to stratigraphically compartmentalise the reservoirs (Cooke-Yarborough 1991; Ketter 1991; Bowman et al. 1993; Hogg et al. 1999), and of the East Irish Sea gas fields, in which aeolian-sandstone layers contribute a disproportionately large amount to flow (Cowan 1993). In these various fields, additional heterogeneities due to faults and burial-related diagenesis, which are not investigated in this study, are also important locally in generating reservoir compartmentalisation, reducing reservoir quality and/or decreasing pressure support and water influx from the aquifer (e.g. Bowman et al. 1993; Meadows & Beach 1993a; Cooke-Yarborough 2003).

By implication, the thickness, lateral continuity and distribution of aeolian sandstones and lacustrine mudstones will control CO_2 plume migration in Sherwood Sandstone Group and Bunter Sandstone Formation storage units. The thickness and stratigraphic position of aeolian-sandstone and lacustrine-mudstone layers can be interpreted from well data, and related to regional changes in climatic aridity during deposition (e.g. Meadows & Beach 1993a; McKie & Williams 2009; Newell 2018a). In depleted oil and gas reservoirs, the lateral extent and distribution of aeolian-sandstone and lacustrine-mudstone layers is likely to be known with confidence, because wells are closely spaced (e.g. McKie et al. 1998; Meadows & Beach 199a; Yaliz & Chapman 2003). In saline aquifers, which are much more sparsely sampled by wells, the lateral extent and distribution of such layers can be inferred with less confidence from regional palaeogeographic reconstructions (e.g. Ziegler 1991; McKie & Williams 2009; Bachmann et al. 2010). For example, aeolian sandstones are interpreted to be absent in the Bunter Sandstone Formation reservoirs of southern North Sea gas fields (Cooke-Yarborough 1991; Ketter 1991; Ritchie & Pratsides 1993), but their presence and potential distribution at the Endurance storage site is uncertain (e.g. Gluyas & Bagudu 2020). Similarly, potential pinchout locations of lacustrine shales in the Endurance storage unit are poorly defined. In the Liverpool Bay depleted gas reservoirs, aeolian-sandstone layers are generally continuous across each field (Meadows & Beach 199a; Yaliz & Chapman 2003; Yaliz & Taylor 2003), but may promote rapid lateral plume migration to, and pressure build-up at, faults that seal reservoir compartments. Thus, key sedimentological uncertainties warrant consideration in the development plans of CO_2 storage sites.

Our results suggest that storage units dominated by laterally continuous aeolian-sandstone bodies are likely to be characterised by rapid and isotropic lateral CO_2 migration through these aeolian-sandstone bodies, but slower migration through intervening facies associations (Figs. 7A, 8, 10). Storage units dominated by laterally continuous lacustrine-mudstone bodies are likely to be compartmentalised across these mudstones (Fig. 7B), thus hindering vertical CO_2 migration. Both heterogeneities may thus promote lateral fingering of a CO_2 plume, with fingers extending through

laterally continuous aeolian sandstones and/or separated by laterally continuous lacustrine mudstones. Such lateral fingering will be accentuated by thin facies-association layers (Figs. 7B, 8). The effect of increasing the lateral continuity of lacustrine-mudstone barriers and baffles is to retain CO_2 within the model volume, and thus to increase storage efficiency. In contrast, increasing the lateral continuity of high-permeability, aeolian-sandstone streaks and thief zones results in reduced CO_2 retention within the model volume, thus decreasing storage efficiency in the absence of barriers to lateral flow such as sealing faults.

CONCLUSIONS

We assess the impact of sedimentological heterogeneity on CO_2 migration and stratigraphic-baffling and trapping potential in the Sherwood Sandstone Group and Bunter Sandstone Formation, UK using a novel and rapid screening methodology that combines experimental design, sketch-based reservoir modelling, and flow diagnostics. Eight heterogeneities were investigated in the screening study: (1) thickness of facies-association layers; lateral continuity of (2) aeolian and (3) lacustrine facies-association bodies; (4) proportion and (5) connectivity of channelised fluvial sandbodies, and (6) lateral continuity of sheetflood sandbodies in floodplain-and-sabkha facies-association layers; and (7) mean vertical spacing and (8) mean lateral extent of carbonate-cemented basal channel lags in fluvial facies-association layers. These heterogeneities vary between Sherwood Sandstone Group and Bunter Sandstone Formation storage units at different prospective CO_2 storage sites, or are uncertain within the storage units. Outcrop and subsurface data were used to constrain values of the investigated heterogeneities. Models represent a small part of a CO_2 storage unit, 600 m x 600 m in areal extent and 176 m thick,, and lack faults and tectonic dip in order to isolate the effects of sedimentological heterogeneity. Flow was simulated between a single injection and a single offtake well.

The lateral continuity of aeolian-sandstone bodies and lacustrine-mudstone bodies, and the thickness of facies-association layers control effective permeability (k_x, k_y, k_z), the Lorenz coefficient, and pore volume injected at breakthrough time (a proxy of the effect of baffles and barriers on CO_2 migration and retention). In addition, k_z is controlled by the mean lateral extent and mean vertical spacing of carbonate-cemented channel lags in fluvial-sandstone layers. Other investigated heterogeneities have only minor influence. These results imply that the distribution and lateral continuity of aeolian sandstones control the direction and rate at which the injected CO_2 plume migrates laterally, while the lateral extent and number of lacustrine-mudstone bodies control vertical plume migration. The effects of these sedimentological heterogeneities should therefore be included in more detailed, future modelling studies of CO_2 migration and storage, particularly where heterogeneity is poorly constrained by well data and hydrocarbon production history in saline aquifers.

ACKNOWLEDGEMENTS

We are grateful for the constructively critical reviews and editorial comments of two anonymous reviewers and Niklas Heinemann. We thank the members of Phase 1 of the Rapid Reservoir Modelling Consortium (Equinor, ExxonMobil Upstream Research Company, Petrobras, Shell, and IBM Research Brazil / IBM Centre for Advanced Studies (CAS) Alberta, Canada) and Phase 2 of the Rapid Reservoir Modelling Consortium (Equinor, ExxonMobil Upstream Research Company, Petrobras, Petronas and Shell) for funding this work and granting permission to publish this paper. SG acknowledges partial funding for his Chair from Energi Simulation. We also thank Will Jackson for practical discussion of sketch-based models presented herein. JA constructed and analysed the models as part of the Petroleum Geoscience MSc course at Imperial College London.

REFERENCES

Agada, S., Kolster, C., Williams, G., Vosper, H., MacDowell, N. & Krevor, S. 2017. Sensitivity analysis of the dynamic CO2 storage capacity estimate for the Bunter Sandstone of the UK Southern North Sea. *Energy Procedia*, **114**, 4564-4570.

Bachmann, G.H., Geluk, M.C., Warrington, G., Becker-Roman, A., Beutler, G., Hagdoen, H., Hounslow, M.W., Nitsch, E., Röhling, H-G., Simon, T. & Szulc, A. 2010. Triassic. *In*: Doornenbal, J.C. & Stevenson, A.G. (eds), *Petroleum Geological Atlas of the Southern Permian Basin Area*, European Association of Geoscientists and Engineers, 149-173.

Bentham, M., Williams, G., Vosper, H., Chadwick, A., Williams, J. & Kirk, K. 2017. Using pressure recovery at a depleted gas field to understand saline aquifer connectivity. *Energy Procedia*, **114**, 2906-2920.

Bentley, M. & Smith, S. 2008. Scenario-based reservoir modelling: the need for more determinism and less anchoring. *In*: Robinson, A., Griffiths, P., Price, S., Hegre, J. & Muggeridge, A. (eds), *The future of geological modelling in hydrocarbon development*. Geological Society of London, Special Publication **309**, 145-159.

Bloomfield, J.P., Moreau, M.F. & Newell, A.J. 2006. Characterization of permeability distributions in six lithofacies from the Helsby and Wilmslow sandstone formations of the Cheshire Basin, UK). *In:* Barker, R.D. & Tellam, J.H. (eds), *Fluid flow and solute movement in sandstones: the onshore UK Permo-Triassic red-bed sequence*, Geological Society of London, Special Publication, **263**, 83-101.

Bowman, M.B.J., McClure, N.M. & Wilkinson, D.W. 1993. Wytch Farm oilfield: deterministic reservoir description of the Triassic Sherwood Sandstone. *In:* Parker, J.R. (ed.), *Petroleum Geology of Northwest Europe: proceeding of the 4th conference*, Geological Society of London, 1513-1517.

Bricker, S.H., Barkwith, A.K.A.P., MacDonald, A.M., Hughes, A.G. & Smith, M. 2012. Effects of CO2 injection on shallow groundwater resources: a hypothetical case study in the Sherwood Sandstone aquifer, UK. *International Journal of Greenhouse Gas Control*, **11**, 337-348.

Brookfield, M.E. 2008. Palaeoenvironments and palaeotectonics of the arid to hyperarid intracontinental latest Permian-late Triassic Solway basin (UK). *Sedimentary Geology*, **210**, 27-47.

Burley, S.D. 1984. Patterns of diagenesis in the Sherwood Sandstone Group (Triassic), United Kingdom. *Clay Minerals*, **19**, 403-440.

Caumon, G., Collon-Drouaillet, P., Le Carlier de Veslud, C., Viseur, S. & Sausse, J. 2009. Surface-based 3D modeling of geological structures. *Mathematical Geosciences*, **41**, 927-945.

Cooke-Yarborough, P. 1991. The Hewett Field, Blocks 48/28-29-30, 52/4a-5a, UK North Sea. *In:* Abbotts, I.L. (ed.), *United Kingdom oil and gas fields: 25 years commemorative volume*, Geological Society of London, Memoir, **14**, 433-442.

Cooke-Yarborough, P. 2003. The Hewett Fields, Blocks 48/28a, 48/29, 48/30, 52/4a, 52/5a, UK North Sea: Hewett, Deborah, Big Dotty, Little Dotty, Della, Dawn and Delilah Fields. *In:* Gluyas, J.G. & Hitchens, H.M. (eds), *United Kingdom oil and gas fields, commemorative millennium volume*, Geological Society of London, Memoir, **20**, 731-739.

Costa Sousa, M., Silva, J.D.M., Silva, C.C.M.M., De Carvalho, F.M., Judice, S., Rahman, F., Jacquemyn, C.E.M.M., Pataki, M.E.H., Hampson, G.J., Jackson, M.D., Petrovskyy, D. & Geiger, S. 2020. Smart modelling of geologic stratigraphy concepts using sketches. *Smart Tools and Applications in computer Graphics (STAG) 2020 Proceedings*, 89-100, https://doi.org/10.2312/stag.20201243

Cowan, G. 1993. Identification and significance of aeolian deposits within the dominantly fluvial Sherwood Sandstone Group of the East Irish Sea Basin UK. *In:* North, C.P. & Prosser, D.J. (eds), *Characterization of fluvial and aeolian reservoirs*, Geological Society of London, Special Publication, **73**, 231-245.

Dranfield, P., Begg, S.H. & Carter, R.R. 1987. Wytch Farm oilfield: reservoir characterization of the Triassic Sherwood Sandstone for input to reservoir simulation studies. *In:* Brooks, J. & Glennie, K.W. (eds), *Petroleum Geology of Northwest Europe*, Graham & Trotman, London, 149-160.

Flett, M., Gurton, R. & Weir, G. 2007. Heterogeneous saline formations for carbon dioxide disposal: impact of varying heterogeneity on containment and trapping. *Journal of Petroleum Science and Engineering*, **57**, 106-118.

Gibson-Poole, C.M., Svendsen, L., Watson, M.N., Daniel, R.F., Ennis-King, J. & Rigg, A.J. 2009. Understanding stratigraphic heterogeneity: a methodology to maximize the efficiency of the geological storage of CO2. *In:* Grobe, M., Pashin, J.C. & Dodge, R.L. (eds), *Carbon dioxide sequestration in geological media – state of the science*, American Association of Petroleum Geologists, Studies in Geology **59**, 347-364.

Gluyas, J.G. & Bagudu, U. 2020. The Endurance CO2 storage site, Blocks 42/25 and 43/21, UK North Sea. *In:* Goffey, G. & Gluyas, J.G. (eds), *United Kingdom oil and gas fields: 50th anniversary commemorative volume*, Geological Society of London, Memoir, **52**, 163-171.

Heinemann, N., Wilkinson, M., Pickup, G.E., Haszeldine, R.S. & Cutler, N.A. 2012. CO2 storage in the offshore UK Bunter Sandstone Formation. *International Journal of Greenhouse Gas Control*, **6**, 210-219.

Hogg, A.J.C., Mitchell, A.W. & Young, S. 1996. Predicting well productivity from grain size analysis and logging while drilling. *Petroleum Geoscience*, **2**, 1-15.

Hogg, A.J.C., Evans, I.J., Harrison, P.F., Meling, T., Smith, G.S., Thompson, S.D. & Watts, G.F.T. 1999. Reservoir management of the Wytch Farm Oil Field, Dorset, UK: providing options for growth into later field life. *In*: Fleet, A.J. & Boldy, S.A.R. (eds), *Petroleum Geology of Northwest Europe: proceeding of the 5th conference*, Geological Society of London, 1157-1172.

Holloway, S., Vincent, C.J., Bentham, M.S. & Kirk, K.L. 2006. Top-down and bottom-up estimates of CO2 storage capacity in the United Kingdom sector of the southern North Sea basin. *Environmental Geosciences*, **13**, 71-84.

Jacquemyn, C., Jackson, M. D. & Hampson, G. J. 2019) Surface-based geological reservoir modelling using grid-free NURBS curves and surfaces. *Mathematical Geosciences*, **51**, 1-28.

Jacquemyn, C.E.M.M., Pataki, M.E.H., Hampson, G.J., Jackson, M.D., Petrovskyy, D., Geiger, S., Silva, J.D.M., Judice, S., Rahman, F., Silva, C.C.M.M. & Costa Sousa, M. 2021a. Sketch-Based Interface and Modelling of Stratigraphy and Structure in 3D. *Journal of the Geological Society of London*, **178**, jgs2020-187.

Jacquemyn, C.E.M.M., Hampson, G.J., Jackson, M.D., Petrovskyy, D., Geiger, S., Silva, J.D.M., Judice, S., Rahman, F. & Costa Sousa, M. 2021b. *Rapid Reservoir Modelling: sketch-based geological modelling with fast flow diagnostics.* Paper SPE 208041, presented at the Abu Dhabi International Petroleum Exhibition and Conference (ADIPEC), Abu Dhabi, 15-18 November.

Jones, N.S. & Ambrose, K. 1994. Triassic sandy braidplain and aeolian sedimentation in the Sherwood Sandstone Group of the Sellafield area, west Cumbria. *Proceedings of the Yorkshire Geological Society*, **50**, 61-76.

Ketter, F.J. 1991. The Esmond, Forbes and Gordon Fields, Blocks 43/8a, 43/13a, 43/15a, 43/20a, UK North Sea. *In:* Abbotts, I.L. (ed.), *United Kingdom oil and gas fields: 25 years commemorative volume*, Geological Society of London, Memoir, **14**, 425-432.

Kirk, K.L. 2005. Potential for storage of carbon dioxide in the rocks beneath the East Irish Sea. *British Geological Survey Internal Report*, **CR/05/127N**, 24 p.

Lorsong, J.A. & Atkinson, C.D. 1995. *Sedimentology and stratigraphy of Lower Triassic alluvial deposits, east Devon coast*. Petroleum Group Excursion Guide, Geological Society of London.

McKie, T., Aggett, J. & Hogg, A.J.C. 1998. Reservoir architecture of the upper Sherwood Sandstone, Wytch Farm field, southern England. *In:* Underhill, J.R. (ed.), *Development, evolution and petroleum geology of the Wessex Basin*, Geological Society of London, Special Publication, **133**, 399-406.

McKie, T. & Williams, B. 2009. Triassic palaeogeography and fluvial dispersal across the northwest European Basins. *Geological Journal*, **44**, 711-741.

Meadows, N.S. 2006. The correlation and sequence architecture of the Ormskirk Sandstone Formation in the Triassic Sherwood Sandstone Group of the East Irish Sea Basin, NW England. *Geological Journal*, **41**, 93-122.

Meadows, N.S. & Beach, A. 1993a. Structural and climatic controls on facies distribution in a mixed fluvial and aeolian reservoir: the Triassic Sherwood Sandstone in the Irish Sea. *In:* North, C.P. & Prosser, D.J. (eds), *Characterisation of fluvial and aeolian reservoirs*, Geological Society of London, Special Publication, **73**, 247-264.

Meadows, N.S. & Beach, A. 1993b. Controls on reservoir quality in the Triassic Sherwood Sandstone of the Irish Sea. *In:* Parker, J.R. (ed.), *Petroleum Geology of Northwest Europe: proceeding of the 4th conference*, Geological Society of London, 823-833.

Medici, G., Boulesteix, K., Mountney, N.P., West, L.J. & Odling, N.E. 2015. Palaeoenvironment of braided fluvial systems in different tectonic realms of the Triassic Sherwood Sandstone Group, UK. *Sedimentary Geology*, **329**, 188-210.

Medici, G., West, L.J. & Mountney, N.P. 2019. Sedimentary flow heterogeneities in the Triassic UK Sherwood Sandstone Group: Insights for hydrocarbon exploration. *Geological Journal*, **54**, 1361-1378.

Monaghan, A., Ford, J., Milodowski, A., McInroy, D., Pharaoh, T., Rushton, J., Browne, M., Cooper, A., Hulbert, A. & Napier, B. 2012. New insights from 3D geological models at analogue CO2 storage sites in Lincolnshire and eastern Scotland, UK. *Proceedings of the Yorkshire Geological Society*, **59**, 53-76.

Morton, A., Hounslow, M.W. & Frei, D. 2013. Heavy-mineral, mineral-chemical and zircon-age constraints on the provenance of Triassic sandstones from the Devon coast, southern Britain. *Geologos*, **19**, 67-85.

Morton, A., Knox, R. & Frei, D. 2016. Heavy mineral and zircon age constraints on provenance of the Sherwood Sandstone Group (Triassic) in the eastern Wessex Basin, UK. *Proceedings of the Geologists' Association*, **127**, 514-526.

Mountney, N.P. & Thompson, D.B. 2002. Stratigraphic evolution and preservation of aeolian dune and damp/wet interdune strata: an example from the Triassic Helsby Sandstone Formation, Cheshire Basin, UK. *Sedimentology*, *49*, 805-833.

Møyner, O., Krogstad, S. & Lie, K.A. 2014. The application of flow diagnostics for reservoir management. *SPE Journal*, **20**, 306-323.

Newell, A.J. 2006. Calcrete as a source of heterogeneity in Triassic fluvial sandstone aquifers (Otter Sandstone Formation, SW England). *In:* Barker, R.D. & Tellam, J.H. (eds), *Fluid flow and solute*

movement in sandstones: the onshore UK Permo-Triassic red-bed sequence, Geological Society of London, Special Publication, **263**, 119-127.

Newell, A.J. 2018a. Evolving stratigraphy of a Middle Triassic fluvial-dominated sheet sandstone: The Otter Sandstone Formation of the Wessex Basin (UK). *Geological Journal*, **53**, 1954-1972.

Newell, A.J. 2018b. Rifts, rivers and climate recovery: a new model for the Triassic of England. *Proceedings of the Geologists' Association*, **129**, 352-371.

Newell, A.J. & Shariatipour, S.M. 2016. Linking outcrop analogue with flow simulation to reduce uncertainty in sub-surface carbon capture and storage: an example from the Sherwood Sandstone Group of the Wessex Basin, UK. *In:* Bowman, M., Smyth, H.R., Good, T.R., Passey, S.R., Hirst, J.P.P. & Jordan, C.J. (eds), *The value of outcrop studies in reducing subsurface uncertainty and risk in hydrocarbon exploration and production*, Geological Society of London, Special Publication, **436**, 231-246.

Noy, D.J., Holloway, S., Chadwick, R.A., Williams, J.D.O., Hannis, S.A. & Lahann, R.W. 2012. Modelling large-scale carbon dioxide injection into the Bunter Sandstone in the UK Southern North Sea. *International Journal of Greenhouse Gas Control*, **9**, 220-233.

Onoja, M.U. & Shariatipour, S.M. 2018. The impact of gradational contact at the reservoir-seal interface on geological CO2 storage capacity and security. *International Journal of Greenhouse Gas Control*, **72**, 1-13.

Onoja, M.U., Williams, J.D., Vosper, H. & Shariatipour, S.M. 2019. Effect of sedimentary heterogeneities in the sealing formation on predictive analysis of geological CO2 storage. *International Journal of Greenhouse Gas Control*, **82**, 229-243.

Petrovskyy, D., Jacquemyn, C.E.M.M., Geiger, S., Jackson, M.D., Hampson, G.J., Silva, J.D.M., Judice, S., Rahman, F. & Costa Sousa, M. in review. Rapid flow diagnostics for reservoir prototyping - applications to subsurface CO2 storage. Submitted to *International Journal of Greenhouse Gas Control*.

Pyrcz, M. J., Catuneanu, O. & Deutsch, C. V. 2005. Stochastic surface-based modeling of turbidite lobes. *AAPG Bulletin*, **89**, 177-191.

Ritchie, J.S. & Pratsides, P. 1993. The Caister Fields, Block 44/23s, UK North Sea. *In:* Parker, J.R. (ed.), *Petroleum Geology of Northwest Europe: proceeding of the 4th conference*, Geological Society of London, 759-769.

Ruiu, J., Caumon, G. & Viseur, S. 2016. Modeling channel forms and related sedimentary objects using a boundary representation based on non-uniform rational B-splines. *Mathematical Geosciences*, **48**, 259-284.

Schmalz, J.P. and Rahme, H.D., 1950. The variation of waterflood performance with variation in permeability profile. *Production Monthly*, **15**, 9-12.

Sech, R.P., Jackson, M.D. & Hampson, G.J. 2009. Three-dimensional modeling of a shoreface-shelf parasequence reservoir analog: part 1. Surface-based modeling to capture high-resolution facies architecture. *American Association of Petroleum Geologists Bulletin*, **93**, 1155-1181.

Shahvali, M., Mallison, B., Wei, K. & Gross, H. 2012. An alternative to streamlines for flow diagnostics on structured and unstructured grids. *SPE Journal*, **17**, 768–778.

Smith, D.J., Noy, D.J., Holloway, S. & Chadwick, R.A. 2011. The impact of boundary conditions on CO2 storage capacity estimation in aquifers. *Energy Procedia*, **4**, 4828-4834.

Tyrrell, S., Haughton, P.D., Souders, A.K., Daly, J.S. & Shannon, P.M. 2012. Large-scale, linked drainage systems in the NW European Triassic: insights from the Pb isotopic composition of detrital K-feldspar. *Journal of the Geological Society*, **169**, 279-295.

Wakefield, O.J., Hough, E. & Peatfield, A.W. 2015. Architectural analysis of a Triassic fluvial system: the Sherwood Sandstone of the East Midlands Shelf, UK. *Sedimentary Geology*, **327**, 1-13.

Williams, J.D.O., Jin, M., Bentham, M., Pickup, G.E., Hannis, S.D. & Mackay, E.J. 2013a. Modelling carbon dioxide storage within closed structures in the UK Bunter Sandstone Formation. *International Journal of Greenhouse Gas Control*, **18**, 38-50.

Williams, J.D.O., Bentham, M., Jin, M., Pickup, G., Mackay, E., Gammer, D. & Green, A. 2013b. The effect of geological structure and heterogeneity on CO2 storage in simple 4-way dip structures; a modeling study from the UK Southern North Sea. *Energy Procedia*, **37**, 3980-3988.

Williams, J.D.O., Holloway, S. & Williams, G.A. 2014. Pressure constraints on the CO2 storage capacity of the saline water-bearing parts of the Bunter Sandstone Formation in the UK Southern North Sea. *Petroleum Geoscience*, **20**, 155-167.

Yaliz, A. and Chapman, T. 2003. The Lennox oil and gas field, block 110/15, East Irish Sea. *In:* Gluyas, J.G. & Hitchens, H.M. (eds), *United Kingdom oil and gas fields, commemorative millennium volume*, Geological Society of London, Memoir, **20**, 87-96.

Yaliz, A. and Taylor, P. 2003. The Hamilton and Hamilton North gas fields, block 110/13a, East Irish Sea. *In:* Gluyas, J.G. & Hitchens, H.M. (eds), *United Kingdom oil and gas fields, commemorative millennium volume*, Geological Society of London, Memoir, **20**, 77-86.

Zhang, Z., Geiger, S., Rood, M.P., Jacquemyn, C.E.M.M., Jackson, M.D., Hampson, G.J., De Carvalho, F.M., Silva, C.C.M.M., Silva, J.D.M. & M. Costa Sousa. 2017. A tracing algorithm for flow diagnostics on fully unstructured grids with multi-point flux approximation. *Society of Petroleum Engineers Journal*, **22**, 1946-1962.

Zhang, Z., Geiger, S., Rood, M.P., Jacquemyn, C.E.M.M., Jackson, M.D., Hampson, G.J., De Carvalho, F.M., Silva, C.C.M.M., Silva, J.D.M. & Costa Sousa, M. 2020. Fast flow computation methods on unstructured tetrahedral meshes for rapid reservoir modelling. *Computational Geosciences*, **24**, 641-661.

Ziegler, P.A. 1991. *Geological Atlas of Western and Central Europe*. Shell Internationale Petroleum Maatschappij B.V., The Hague.

Figure Captions

Fig. 1

Map locating Sherwood Sandstone Group outcrops of the onshore UK, offshore CO_2 storage sites currently being appraised in the East Irish Sea and southern North Sea, and the Wytch Farm oil field.

Fig. 2

Interpreted hierarchy of heterogeneities across a range of length scales within the predominantly fluvial and aeolian deposits of the Sherwood Sandstone Group and Bunter Sandstone Formation, and the lacustrine deposits of the overlying Mercia Mudstone Group and Haisborough Group: (**A**) cross-section illustrating basin-scale interfingering of lithostratigraphic units that form the CO_2 storage complex (after McKie & Williams 2009; Newell 2018a, 2018b); (**B**) cross-section illustrating reservoir-scale interfingering of fluvial, aeolian, floodplain/sabkha and lacustrine facies associations that form the CO_2 storage unit (Fig. 3A) (after McKie et al. 1998; Yaliz & Chapman 2003; Meadows 2006; Newell 2018a); (**C**) cross-section illustrating stacking of channelised sandbodies within a multistorey fluvial facies association, including carbonate-cemented basal channel lags (Fig. 3A-B) and incompletely preserved channel-fill successions (Fig. 3C) (after Bowman et al. 1993; McKie et al. 1998; Medici et al. 2015; Newell 2018a). Smaller-scale heterogeneities related to facies, sedimentary structures, and sandstone texture are not shown.

Fig. 3

Photographs of selected heterogeneities in the Sherwood Sandstone Group at outcrop in the south coast of Devon, England (Fig. 1). (**A**) Fluvial-sandstone layer, characterised by multistorey and multilateral stacking of channelised fluvial sandbodies, overlain (across dotted white line) by layer of floodplain and sabkha heteroliths, which consists of channelised fluvial sandbodies and non-channelised sheetflood sandbodies interbedded with mudstones (Fig. 2B). Resistant, carbonate-cemented lags at the base of channelised fluvial sandbodies (Fig. 2C) are indicated by blue arrows. (**B**) Vertically stacked, partially preserved, channelised fluvial sandbodies in a fluvial-sandstone layer. Each channelised sandbody has a carbonate-cemented lag at its base (indicated by blue arrows), overlain by high-angle cross-beds and then low-angle cross-strata (Fig. 2C). (**C**) Mudstone channel plug in a fluvial-sandstone layer (Fig. 2C). (**D**) Thick, channelised fluvial sandbodies and thin, non-channelised sheetflood sandbodies interbedded with mudstones in a layer of floodplain and sabkha heteroliths (Fig. 2B). Photographs are taken from Ladram Bay (Fig. 3A-C) and Sidmouth East Cliff (Fig. 3D).

Fig. 4

3D perspective views of a representative model showing: (**A**) sketch-generated surfaces; (**B**) surface-bounded geological domains; and (**C**) well placements for south-to-north tracer flow (blue) and west-to-east tracer flow (red). Model grids are shown for visualisation purposes only.

Fig. 5

3D perspective views of selected models, illustrating contrasting stratigraphic architectures that result from combinations of the settings for different heterogeneities (Table 1): (**A**) model number 28, characterised by thick facies-association layers, laterally continuous aeolian-sandstone sheets, laterally discontinuous lacustrine-mudstone sheets, many and relatively poorly connected channelised fluvial sandbodies and discontinuous sheetflood sandbodies in floodplain-and-sabkha-heterolith layers (Table 2); (**B**) model number 22, characterised by thick facies-association layers, laterally discontinuous aeolian-sandstone lenses, laterally continuous lacustrine-mudstone sheets, few and well connected channelised fluvial sandbodies and discontinuous sheetflood sandbodies in floodplain-and-sabkha-heterolith layers (Table 2); and (**C**) model number 15, characterised by thin facies-association layers, laterally continuous aeolian-sandstone sheets and lacustrine-mudstone sheets, many and relatively poorly connected channelised fluvial sandbodies and continuous sheetflood sandbodies in floodplain-and-sabkha-heterolith layers (Table 2). See Figure 4 for key to facies association colours, but note that channelised fluvial sandbodies in different floodplain-and-sabkha-heterolith layers are assigned different colours in Fig. 5C, to help with their identification during model construction and quality checking. Fluvial sandstones in between laterally discontinuous aeolian-sandstone lenses are not visualised in Fig. 5B, so that the geometry of the latter can be seen.

Fig. 6

Tornado chart showing the average percentage changes in total pore volume that result from varying each sedimentological heterogeneity (factor) from its low setting to its high setting (Table 1). If the bar lies to the right then the change is positive. For example, modelling discontinuous lenses of aeolian sandstone (low setting) increases total pore volume by *c.* 7% compared with modelling continuous aeolian-sandstone sheets (high setting). The largest response of confounded 2-factor interactions is shown for comparison with the main effects due to individual factors. Changes in total pore volume are small (<7%) for all factors.

Fig. 7

Tornado charts showing the average percentage changes in (**A**) effective horizontal permeability in west-east (k_x) and north-south (k_y) orientations, and (**B**) effective vertical permeability (k_z) that result

from varying each factor from its low setting to its high setting (Table 1). If the bar lies to the right then the change is positive. For each tornado chart, the largest response of confounded 2-factor interactions is shown for comparison with the main effects due to individual factors.

Fig. 8

Tornado chart showing the average percentage changes in Lorenz coefficient that result from varying each factor from its low setting to its high setting (Table 1). If the bar lies to the right then the change is positive. The largest response of confounded 2-factor interactions is shown for comparison with the main effects due to individual factors.

Fig. 9

Tornado chart showing the average percentage changes in pore volume injected at breakthrough time that result from varying each factor from its low setting to its high setting (Table 1). If the bar lies to the right then the change is positive. The largest response of confounded 2-factor interactions is shown for comparison with the main effects due to individual factors.

Fig. 10

3D perspective views of model number 2 (Table 2) showing: (**A**) facies-association distributions and well placements for west-to-east tracer flow; (**B**) facies-association distributions with fluvial sandstones not visualised, in order to highlight the geometry and position of laterally discontinuous aeolian sandstones; and (**C-F**) simulated tracer flow for progressively increased durations of time-of-flight from the injector well. (**C**) Tracer is injected into sheetflood, fluvial and aeolian sandstones, (**D**) flows preferentially through two laterally discontinuous aeolian sandstones to their eastern pinchouts, (**E**) breaks through at the offtake well via two more easterly, laterally discontinuous aeolian sandstones, and (**F**) sweeps through remaining aeolian and fluvial sandstones. Tracer breakthrough at the offtake well occurs at 0.45 pore volumes injected (PVI).

Table Captions

Table 1

Summary of investigated sedimentological heterogeneities (factors) and their low and high settings in the screening study. The impact of these eight factors on simulated fluid flow is assessed by observing the percentage change in average response when each factor is varied from its low setting to its high setting.

Table 2

Design and parameter settings (l = low, h = high; Table 1) in the 32 models constructed for the screening study.

Table 3

Porosity and permeability values assigned to each facies association represented in the models (Fig. 2B).

Sedimentological heterogeneity (factor)	**Low setting**	**High setting**
thickness of facies-association layers	thin (fluvial: 10 m, aeolian: 5 m, floodplain/sabkha: 5 m, lacustrine: 2 m)	thick (fluvial: 40 m, aeolian: 25 m, floodplain/sabkha: 20 m, lacustrine: 5 m)
lateral continuity of aeolian facies-association bodies	discontinuous lense	continuous sheet
lateral continuity of lacustrine facies-association bodies	discontinuous sheet	continuous sheet
proportion of channelised fluvial sandbodies in floodplain/sabkha facies-association layers	low (c. 17%)	high (c. 33%)
lateral connectivity of channelised fluvial sandbodies in floodplain/sabkha facies-association layers	isolated clusters of channelised sandbodies	connected network of channelised sandbodies
lateral continuity of sheetflood sandbodies in floodplain/sabkha facies-association layers	continuous sheet	discontinuous lense
mean vertical spacing of carbonate-cemented basal channel lags in fluvial facies-association layers	2 m	10 m
mean lateral extent of carbonate-cemented basal channel lags in fluvial facies-association layers	8 m	20 m

Table 1

Sedimentological heterogeneity (factor)	Model number																															
	1	**2**	**3**	**4**	**5**	**6**	**7**	**8**	**9**	**10**	**11**	**12**	**13**	**14**	**15**	**16**	**17**	**18**	**19**	**20**	**21**	**22**	**23**	**24**	**25**	**26**	**27**	**28**	**29**	**30**	**31**	**32**
thickness of facies-association layers	l	h	l	h	l	h	l	h	l	l	l	h	l	h	l	h	l	h	l	h	l	h	l	h	l	h	l	h	l	h	l	h
lateral continuity of aeolian facies-association bodies	l	l	h	h	l	l	h	h	l	l	h	h	l	l	h	h	l	l	h	h	l	l	h	h	l	l	h	h	l	l	h	h
lateral continuity of lacustrine facies-association bodies	l	l	l	l	h	h	h	h	l	l	l	l	h	h	h	h	l	l	l	l	h	h	h	h	l	l	l	l	h	h	h	h
proportion of channelised fluvial sandbodies in floodplain/sabkha facies-association layers	l	l	l	l	l	l	l	l	h	h	h	h	h	h	h	h	l	l	l	l	l	l	l	l	h	h	h	h	h	h	h	h
lateral connectivity of channelised fluvial sandbodies in floodplain/sabkha facies-association layers	h	h	l	l	l	l	h	h	l	l	h	h	h	h	l	l	l	l	h	h	h	h	l	l	h	h	l	l	l	l	h	h
lateral continuity of sheetflood sandbodies in floodplain/sabkha facies-association layers	l	l	l	l	l	l	l	l	l	l	l	l	l	l	l	l	h	h	h	h	h	h	h	h	h	h	h	h	h	h	h	h
mean vertical spacing of carbonate-cemented basal channel lags in fluvial facies-association layers	l	h	h	l	l	h	h	l	h	l	l	h	h	l	l	h	l	h	h	l	l	h	h	l	h	l	l	h	h	l	l	h
mean lateral extent of carbonate-cemented basal channel lags in fluvial facies-association layers	l	h	h	l	h	l	l	h	l	h	h	l	h	l	l	h	l	h	h	l	h	l	l	h	l	h	h	l	h	l	l	h

Table 2

facies sssociation	porosity (%)	permeability (mD)
aeolian sandstone	24	3000
fluvial sandstone	17	500
sheetflood sandstone	15	200
floodplain and sabkha mudstone	5	1
lacustrine mudstone	7	1

Table 3

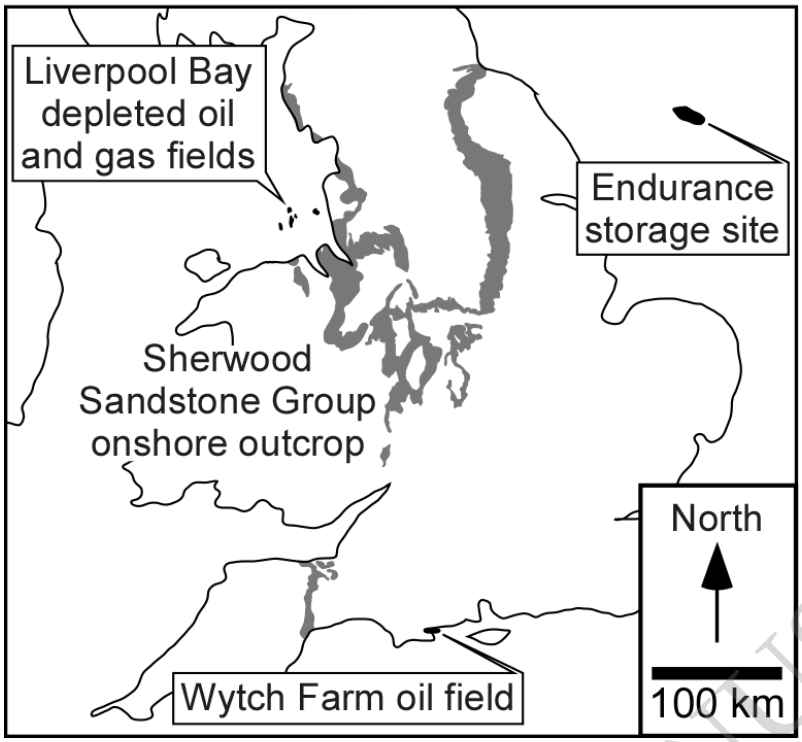

Figure 1

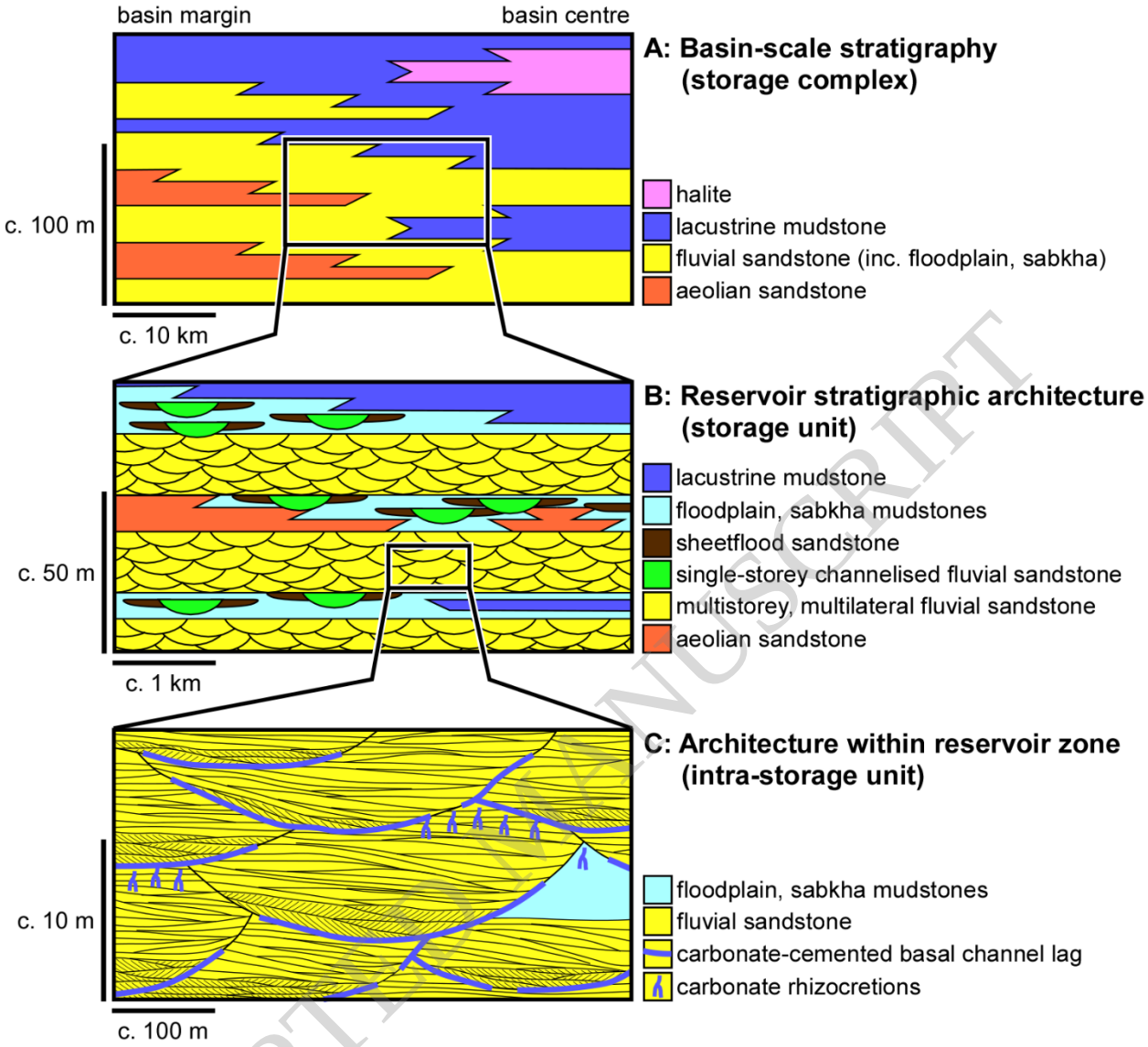

Figure 2

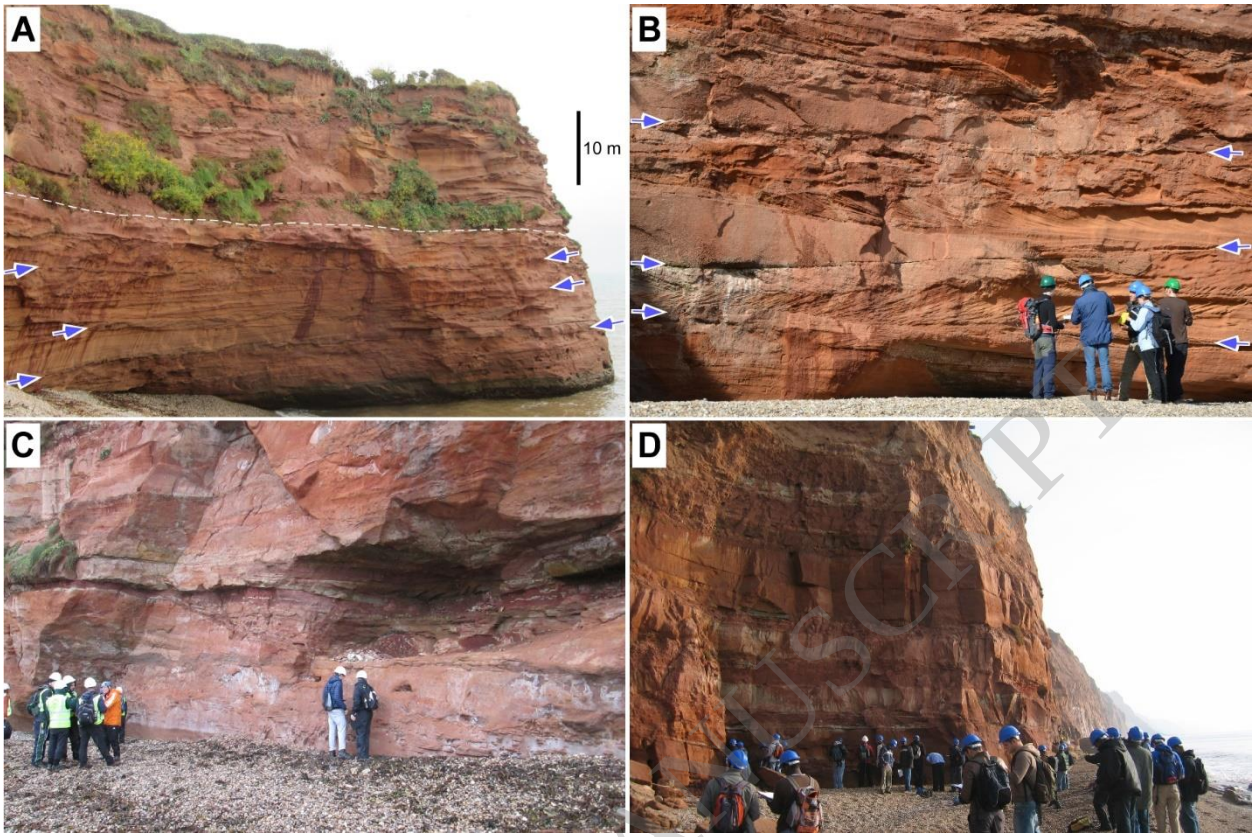

Figure 3

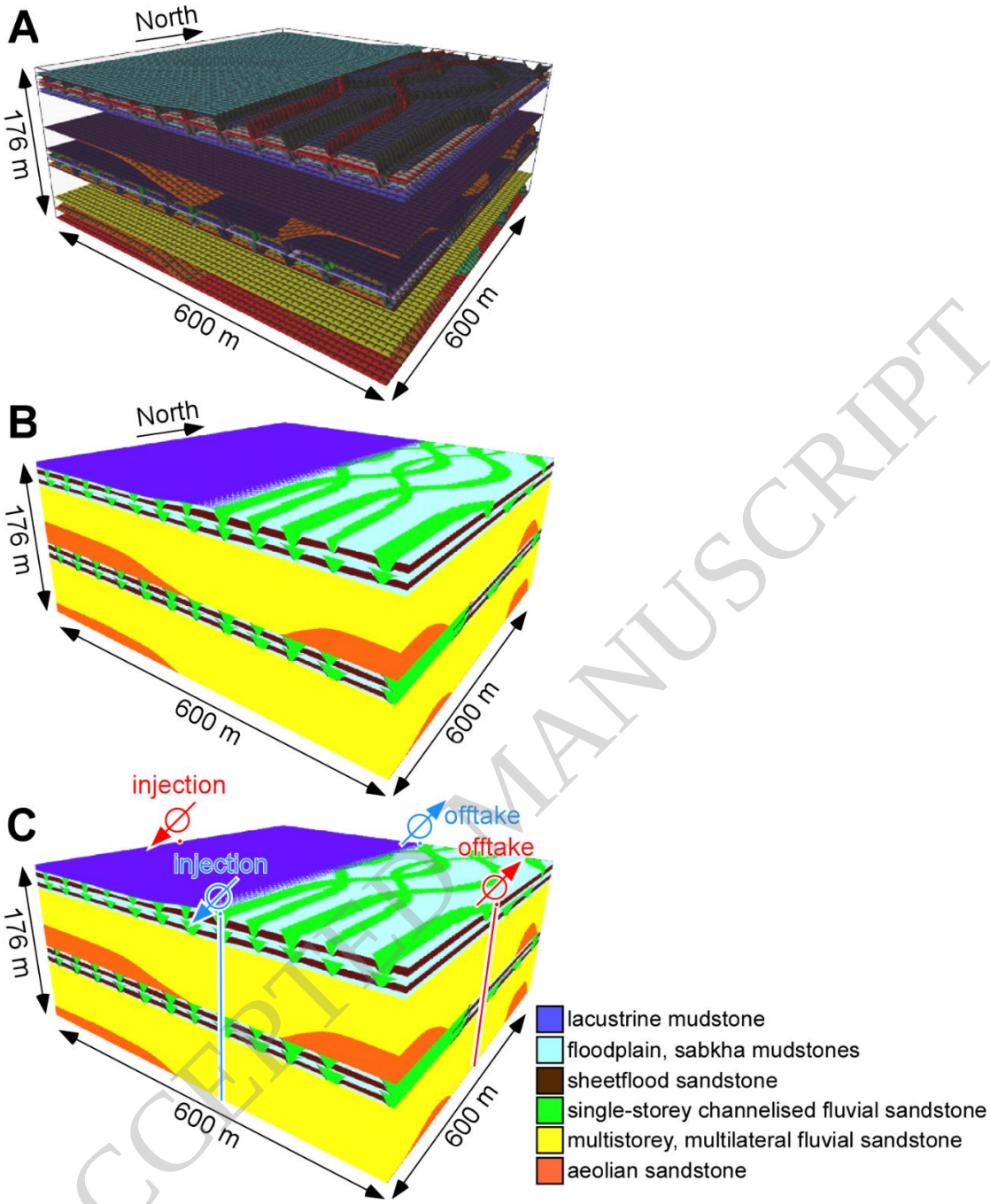

Figure 4

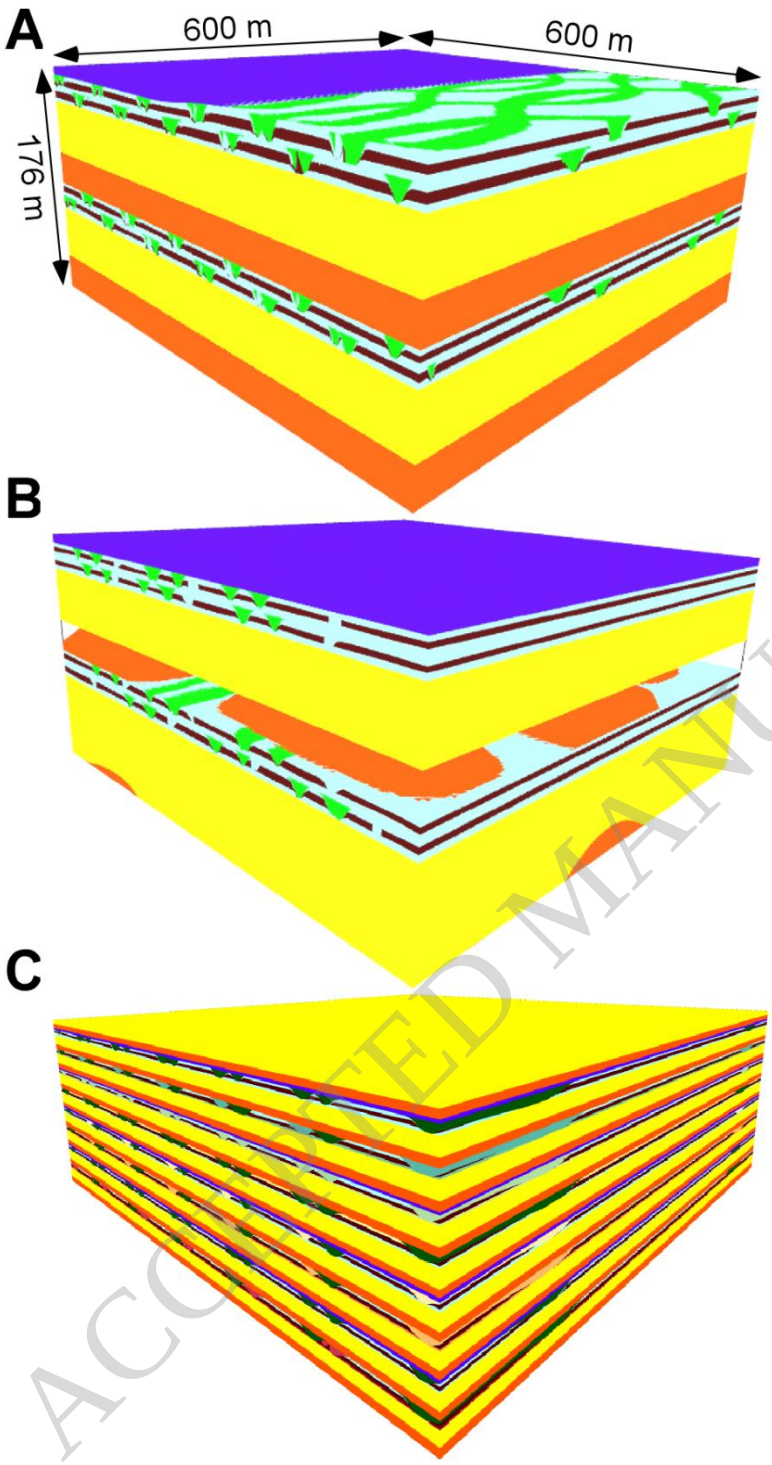

Figure 5

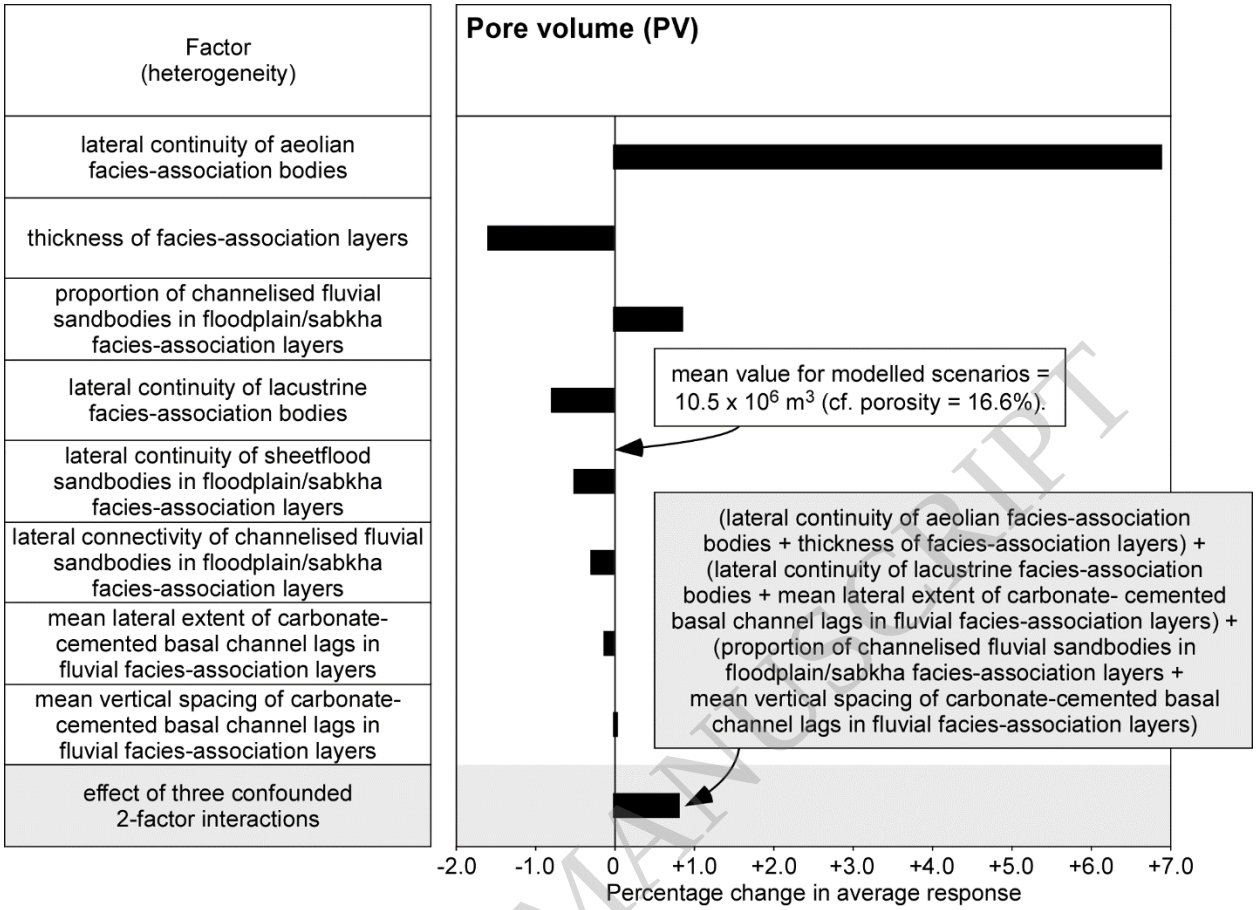

Figure 6

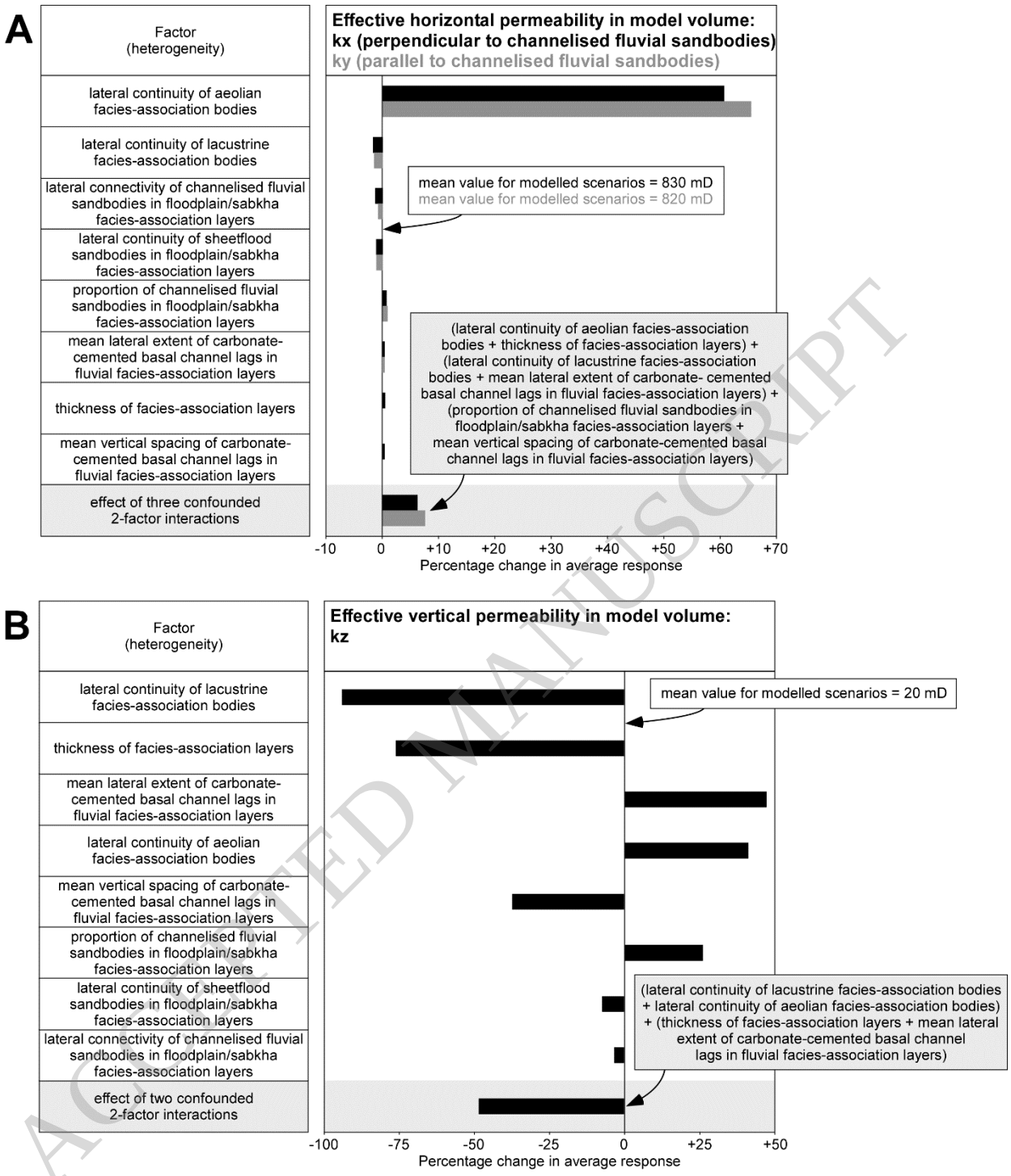

Figure 7

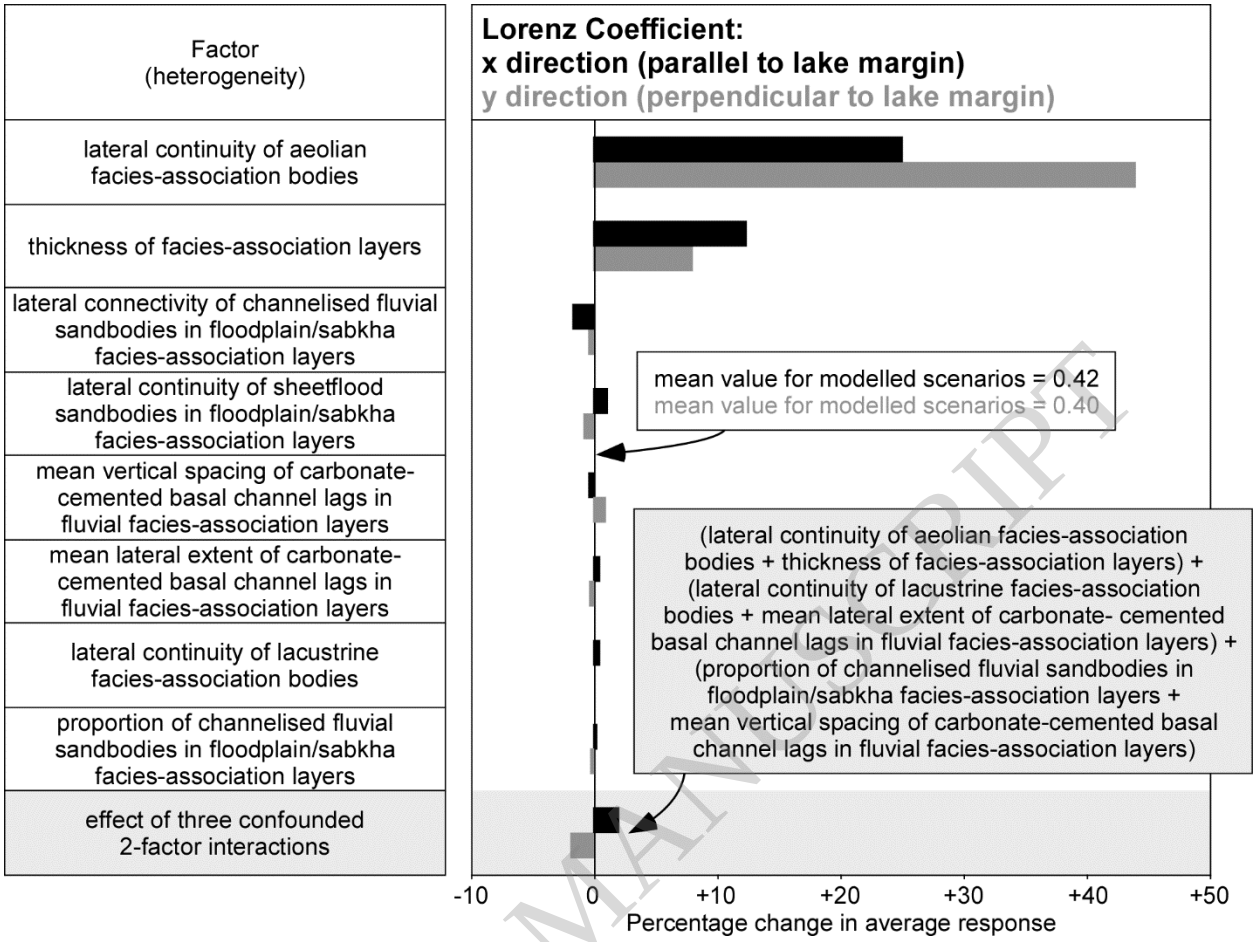

Figure 8

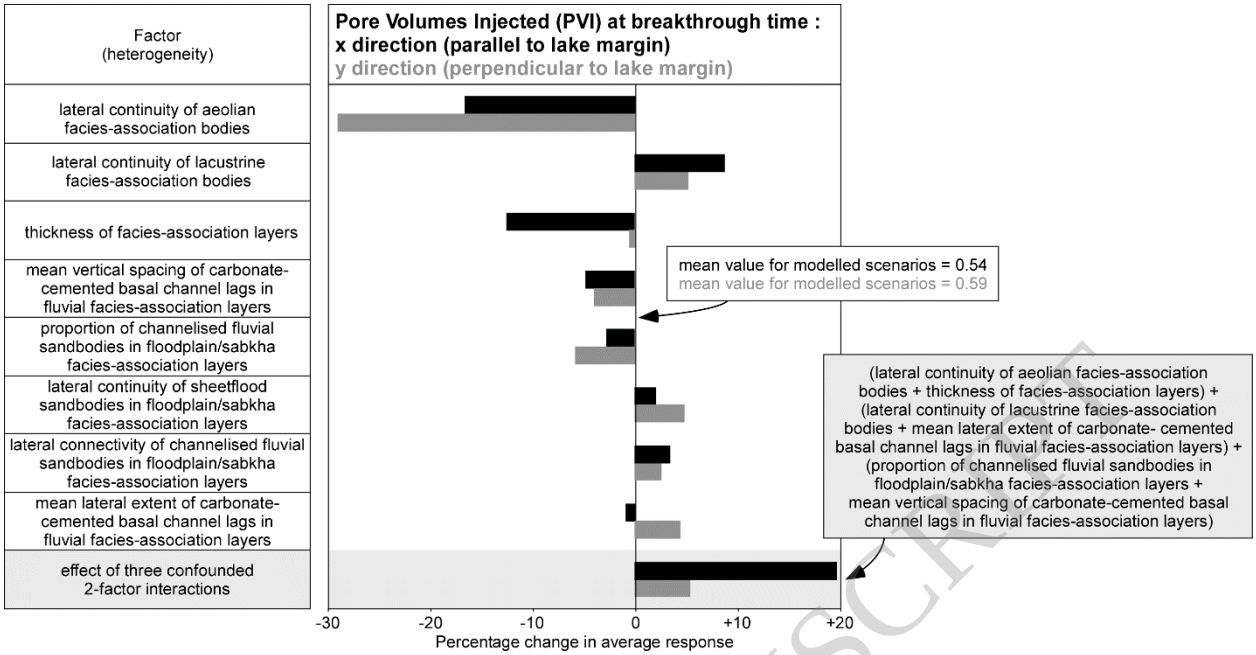

Figure 9

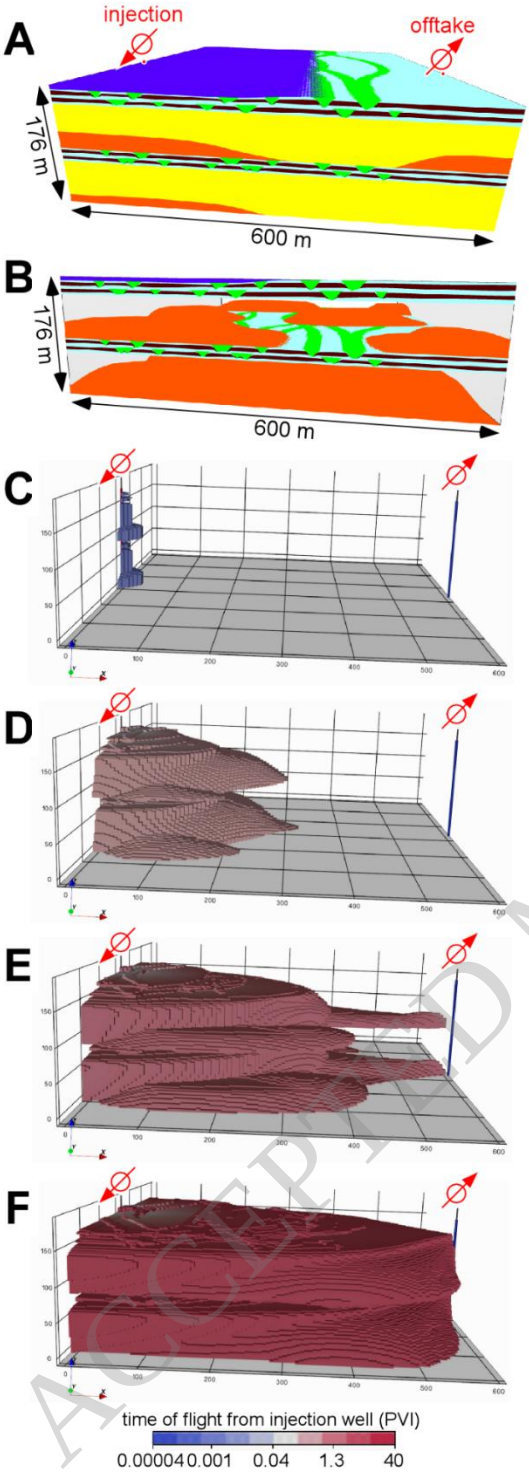

Figure 10